ACS OMEGA

Open Access



http://pubs.acs.org/journal/acsodf

Article

# Development and Optimization of Piracetam and Shatavarin IV-Loaded Nanoemulsion for Alzheimer's Disease Therapy: In Silico and Experimental Analysis

Mohd Nadeem, Haya Majid, Mohd Danish Ansari, Farhan Jalees Ahmad, Suhel Parvez, Mohd Akhtar, Sayeed Ahmad, and Abul Kalam Najmi*

Cite This: *ACS Omega* 2025, 10, 9132−9153

Read Online

ACCESS | Metrics & More | Article Recommendations

**ABSTRACT:** Alzheimer's disease (AD) presents a significant challenge due to cognitive decline resulting from nerve cell degeneration. Shatavarin IV, a prominent bioactive compound from*Asparagus racemosus* and Piracetam, has been investigated for its neuroprotective potential. This study examines the molecular docking, formulation, and characterization of a nanoemulsion containing Piracetam and Shatavarin IV for treating AD. The *in silico* study demonstrated that Shatavarin IV exhibited strong binding affinities with multiple AD-related targets, including TNF-$\alpha$ (−7.29 kcal/mol), the GSK-3 axin complex (−9.6785 kcal/mol), amyloid-$\beta$ (−6.8326 kcal/mol), and GSK-3 $\beta$ (−8.8243 kcal/mol). The extraction of Shatavarin IV from *Asparagus racemosus* roots yielded 401.1 ± 2.3 mg with a purity of 66%, as confirmed by HPTLC. A combination index study revealed a synergistic effect with a CI value of 0.10843 at a 1:1 ratio of Piracetam and Shatavarin IV. The nanoemulsion was optimized using a Box-Behnken design, with oil concentration, surfactant mixture ($S_{mix}$), and sonication time as key factors. The optimized formulation exhibited a particle size of 183.6 nm and a PDI of 0.194. Characterization techniques, including TEM and DSC, confirmed the uniformity, stability, and incorporation of the drugs in the nanoemulsion. The *in vitro* drug release study revealed a significantly higher release profile (84.30 ± 1.03% in 24 h) for the nanoemulsion than the drug suspension. *Ex vivo* studies demonstrated a superior permeability rate for the nanoemulsion (56.35 ± 1.19%) compared to the conventional suspension. Additionally, the nanoemulsion showed enhanced antioxidant activity compared with the pure extract. Stability studies indicated that the formulation remained stable with only minor changes in particle size, PDI, and zeta potential over time. This nanoemulsion presents a promising therapeutic strategy for AD.

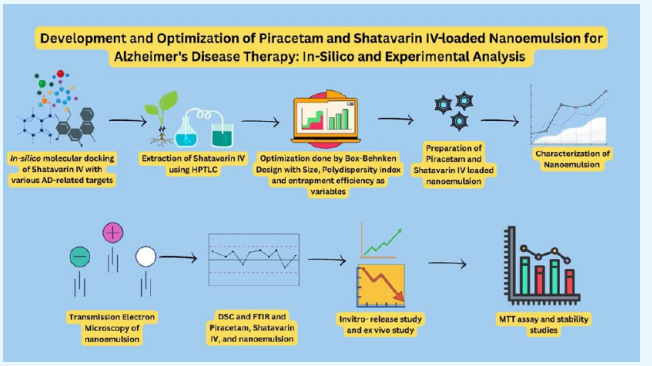


## 1. INTRODUCTION

Alzheimer's disease (AD) remains the most prevalent form of dementia, characterized by progressive memory and cognitive decline due to nerve cell degeneration. Its global impact is substantial, with projections indicating a tripling of affected individuals to around 150 million by 2050, particularly in low- and middle-income countries.[1] Furthermore, dementia prevalence in Europe is expected to double by 2050.[2] The distinctive features of AD encompass amyloid-beta (A$\beta$) plaque accumulation, neurofibrillary tangle (NFT) formation, inflammation, and neuronal loss in specific brain regions, culminating in cognitive decline and impaired daily functioning.[3,4]

Existing treatments for AD focus on symptom management rather than addressing the underlying neurodegenerative processes.[3] Current anti-AD medications, including cholinesterase inhibitors (donepezil, rivastigmine, and galantamine) and *N*-methyl-D-aspartate (NMDA) receptor antagonists (memantine), provide only limited benefits and are primarily focused on managing symptoms rather than altering the course of the disease.[5] Current medications only offer modest improvements in cognitive and functional symptoms, and their benefits often diminish over time.[6,7] Many patients experience adverse side effects, such as gastrointestinal disturbances, dizziness, and cardiovascular effects, which can limit their tolerability and long-term use. These side effects often lead to discontinuation of therapy, reducing overall treatment adherence.[8,9] To address this, herbal remedies have been investigated to address behavioral and psychological

Received: October 4, 2024
Revised: February 13, 2025
Accepted: February 14, 2025
Published: February 24, 2025

symptoms of dementia (BPSD), with varying responses.[10,11] Despite their rich traditional use and perceived safety, scientific exploration of these remedies has been limited.[12,13] Traditional medicinal practices suggest various herbs and components to improve cognitive function and manage AD-related symptoms, tailored to the condition's severity.[14]

Shatavarin IV is a primary bioactive compound in *Asparagus racemosus*, also known as Shatavari, a perennial herb widely used in traditional Ayurvedic medicine. This compound is classified as a steroidal saponin, which contributes significantly to the medicinal properties attributed to Shatavari. Shatavarin IV is believed to exert neuroprotective effects through several mechanisms that may be beneficial in AD.[15] One of the primary actions of Shatavarin IV is its antioxidant capacity, which helps reduce oxidative stress — a significant contributor to neuronal damage in AD patients. By scavenging free radicals and enhancing the activity of endogenous antioxidant enzymes, Shatavarin IV may help protect neuronal cells from oxidative damage, thereby slowing the progression of neurodegeneration.[16] Additionally, Shatavarin IV has shown potential anti-inflammatory properties, which could be beneficial in managing AD by reducing the production of pro-inflammatory cytokines that contribute to neuronal damage.[17,18] By mitigating inflammation, Shatavarin IV could help preserve neuronal function and structure, potentially slowing cognitive decline.[19] While Shatavarin IV shows promise in managing AD through its neuroprotective properties, it may not be sufficient on its own to produce significant therapeutic efficacy in the advanced stages of the disease.[20] Thus, while Shatavarin IV may help mitigate some of these factors, combining it with other agents could enhance its overall impact on the disease.[21] The addition of Piracetam, a nootropic agent widely recognized for its cognitive-enhancing effects, could complement the actions of Shatavarin IV and provide a more robust therapeutic approach for AD.[22−24] Piracetam is known to enhance neuronal function by improving membrane fluidity, increasing mitochondrial function, and enhancing cerebral blood flow.[25] It also modulates neurotransmitter release, particularly acetylcholine, which is crucial for cognitive processes like memory and learning that are severely impaired in AD patients.[26] Moreover, Piracetam has been shown to have neuroprotective properties. It may protect neurons from various forms of damage, such as those caused by oxidative stress, hypoxia (low oxygen), and neurotoxicity.[27] Additionally, it is thought to improve microcirculation in the brain without causing vasodilation, which can help enhance cognitive function, especially in individuals with cognitive impairments related to aging or neurodegenerative conditions.[28] Clinically, Piracetam is used in several countries (although not approved in the U.S. by the FDA) to treat cognitive disorders, including AD, age-related cognitive decline, and poststroke cognitive deficits. It has also been explored in conditions such as dyslexia, vertigo, and myoclonus. While its safety profile is generally considered favorable, with few side effects, its effectiveness can vary depending on the condition being treated, and more research is needed to understand its full range of effects and potential benefits.[24,29,30]

The combination of Shatavarin IV and Piracetam could offer a synergistic effect in addressing the multifactorial nature of AD. While Shatavarin IV targets oxidative stress and inflammation, Piracetam could enhance cognitive functions by directly improving neuronal communication and synaptic plasticity. This dual action might provide a more comprehensive neuroprotective strategy, potentially slowing disease progression and improving cognitive outcomes in patients. Furthermore, Piracetam's role in neuroprotection may help potentiate the beneficial effects of Shatavarin IV, offering a combined therapeutic strategy that is greater than the sum of its parts.

A nanoemulsion formulation offers several advantages that could significantly enhance the therapeutic efficacy of the combination of Shatavarin IV and Piracetam in the management of AD. Nanoemulsions are colloidal dispersions of two immiscible liquids, typically oil and water, stabilized by surfactants. These formulations are characterized by their small droplet size, usually ranging from 20 to 200 nanometers, which provides unique properties that can improve drug delivery, especially for compounds with poor water solubility, such as Shatavarin IV.[31−33] The use of a nanoemulsion for delivering Piracetam and Shatavarin IV can enhance their bioavailability by improving their solubility and absorption. Nanoemulsions can increase the surface area available for absorption in the gastrointestinal tract, promoting a better uptake of both compounds into the systemic circulation. This is particularly beneficial for Shatavarin IV, which has limited solubility in water and may otherwise have poor bioavailability when administered in conventional forms. Enhanced solubility and stability of the nanoemulsified drugs can also reduce the required dosage, minimizing potential side effects and improving patient compliance.[34−36]

Additionally, nanoemulsions can facilitate targeted delivery to the brain, a critical factor in treating AD. The small droplet size allows the nanoemulsion to cross biological barriers more efficiently, including the blood−brain barrier (BBB), which is a significant challenge for many therapeutic agents. By penetrating the BBB more effectively, the nanoemulsion can deliver higher concentrations of Shatavarin IV and Piracetam directly to the site of action, potentially enhancing their neuroprotective effects and cognitive benefits.[37,38] Furthermore, nanoemulsions can protect the active compounds from degradation by enzymes or environmental factors, prolonging their stability and maintaining their therapeutic potency. This is particularly important for Shatavarin IV, which may degrade quickly in the gastrointestinal tract or under physiological conditions. Encapsulation within a nanoemulsion can shield these compounds, ensuring sustained and controlled release over time, which may lead to prolonged therapeutic effects and improved management of AD symptoms.[32,34,36,38]

This study addresses these gaps by developing a novel nanoemulsion to enhance the bioavailability of Shatavarin IV and Piracetam, leveraging their synergistic effects to target AD's multifactorial pathology. The rationale of the optimized formulation is to improve drug solubility, stability, and brain permeability, offering a promising therapeutic strategy to overcome the limitations of the current treatments. The present study aims to observe *in silico* binding efficacy, *in vitro* optimization, and characterization of Piracetam and Shatavarin IV nanoemulsion (PSNE).

## 2. MATERIALS AND METHODS

Shatavarin (*A. racemosus*) roots were obtained from Universal Biotech, India, and were validated by a botanist of the Department of Botany, School of Chemical and Life Sciences, Jamia Hamdard, New Delhi, India, with reference no. BOT/DAC/2021/08. Piracetam (batch no. DY0301901036) was kindly gifted by Sun Pharmaceuticals Pvt. Ltd., India. The



https://doi.org/10.1021/acsomega.4c09072
ACS Omega 2025, 10, 9132−9153

reference standard of Shatavarin IV was obtained from Natural Remedies Pvt. Ltd., Bangalore. Other chemicals such as Tween 80, Capmul MCM C8, Transcutol P, Poloxamer 88, span 80, ethanol, propylene glycol, distilled water, Pluronic F-68, potassium sorbate, and hydrochloric acid were purchased from Sigma Merck, USA. Methanol, *n*-hexane, ethyl acetate, chloroform, *n*-butanol, and formic acid were procured from Goyal Chemicals Co., Pvt. Ltd., India.

**2.1. *In Silico* Study.** The binding affinity of Shatavarin IV with various AD-related targets, including TNF-$\alpha$ (PDB ID: 2AZ5), GSK-3 axin complex (PDB ID: 4NM0), GSK-3 $\beta$ complex (PDB ID: 1H8F), and A$\beta$ (PDB ID: 4Q8D), was evaluated using Molecular Operating Environment (MOE) 2015.10. These computational studies were conducted on a Windows 10-based Asus desktop computer equipped with a 64-bit operating system, an Intel Core i3 processor, a 4 GB Intel graphics card, and 16 GB of RAM. The ligand preparation process began by generating the structure of Shatavarin IV using ChemDraw Tool version 16.0 in CDX format, which was then converted into Mol-SD file format. The energy minimization of the ligand was performed in MOE, and the minimized structure was saved in .mdb format for further molecular docking studies. The crystal structures of the target proteins were obtained from the RCSB Protein Data Bank (https://www.rcsb.org/). The proteins were prepared by using the QuickPrep protocol in MOE, followed by active site selection using Site Finder, which was converted into dummy atoms for docking. The receptor−ligand docking was performed using the Dock module, and the ligand molecules were docked into the receptor's binding site. The docking analysis used the S score as the assessment metric to evaluate the favorable interactions between the ligand molecules and the receptor. Molecules with a binding energy lower than −6.0 kcal/mol were considered for further investigation.

**2.2. Extraction.** The tuberous roots of *A. racemosus* (250 g) were finely powdered. The powdered root material was then defatted using hexane to remove the lipid content. After defatting, the remaining powder was subjected to maceration, where it was extracted multiple times with 90% methanol at room temperature over 24 h. The total methanolic extract obtained was concentrated by evaporation by using a water bath. The mass of the concentrated extract was then recorded, and the percentage yield was calculated based on the initial weight of the plant material. The concentrated extract was subsequently stored in an airtight container for further analysis and research.[39,40]

*2.2.1. Analysis of Methanolic Extract (A. racemosus Root) Using High-Performance Thin-Layer Chromatography Profiling and Quantitative Estimation.* In the analysis of the methanolic extract of *A. racemosus* roots, 30 mg of the extract was dissolved in HPLC-grade methanol and filtered through a 0.2 $\mu$M polytetrafluoroethylene (PTFE) membrane filter. From this stock solution, the extract was further diluted to achieve a final concentration of 0.5 mg/mL. Using the Camag Linomat-V applicator (CAMAG, Switzerland), 6 $\mu$L of the prepared sample was applied onto prewashed and activated Silica gel 60 F254 precoated HPTLC plates (10 × 10 cm, Merck, Germany). The sample was applied as a 6 mm wide band with nitrogen flow controlling the delivery speed at 150 nL/s. To achieve the optimal separation and resolution of Shatavarin IV and other metabolites, several solvent systems were evaluated during HPTLC profiling. The combinations tested included ethyl acetate: methanol: formic acid (7.5:2:0.5, v/v), ethyl acetate: methanol (7.5:2.5, v/v), chloroform: methanol (7:3, v/v), and chloroform: methanol: formic acid (7:2.5:0.5, v/v). Among these, the solvent system was ethyl acetate: methanol: formic acid (7.5:2:0.5, v/v) was identified as optimal based on its ability to provide well-defined, sharp, and reproducible bands with consistent $R_f$ values for Shatavarin IV (0.45 ± 0.05). This optimized solvent system was used for all subsequent quantitative estimations, ensuring accuracy and reproducibility of the analysis. The development was carried out at room temperature (25 °C) over a distance of 80 mm. After development, one plate was dried and visualized under visible light (white), short-wave UV light (254 nm), and long-wave UV light (366 nm) to observe the separation of the compounds. For another plate, an anisaldehyde-sulfuric acid reagent was sprayed, and the plate was heated for 5 min at 100 °C to induce color development, highlighting the phytochemical constituents. The HPTLC method for analyzing Shatavarin IV in the methanolic extract of *A. racemosus* root was developed and validated following ICH Q2(R1) guidelines. Specificity was ensured by resolving Shatavarin IV ($R_f$ = 0.45 ± 0.05) without interference from other components. Linearity was demonstrated with a calibration curve (1−25 $\mu$g/mL) yielding a regression equation of $y = 71.507x + 1976.916$ and $r^2 = 0.98842$. Accuracy was confirmed through recovery studies (98.5%−101.2%), and precision showed % RSD values below 2.0% for intra- and interday variability. The method's sensitivity was validated with LOD and LOQ values of 0.2 and 0.5 $\mu$g/mL, respectively. Robustness testing under altered conditions (mobile phase composition and detection wavelength) confirmed method consistency, and analyte stability was validated over 48 h. Using the optimized mobile phase (ethyl acetate: methanol: formic acid, 7.5:2:0.5, v/v), samples were applied to precoated silica gel plates, developed, and scanned at 254 nm with WINCATS 1.2.3 software. These results affirm the method's reliability and reproducibility for quantitative estimation of Shatavarin IV.[41−43]

*2.2.2. Identification and Estimation of Shatavarin IV.* To identify and quantify Shatavarin IV, HPTLC was utilized. Both the isolated fractions and the final dried extract were analyzed by using this method. Standard Shatavarin IV and the isolated compound were each dissolved in methanol to prepare stock solutions of 100 $\mu$g/mL. From these solutions, 16 $\mu$L of each sample and the standard solution were applied to a Silica gel 60 F254 precoated plate (0.25 mm thickness) using a CAMAG Linomat V applicator. The chromatographic separation was carried out using a mobile phase consisting of ethyl acetate: methanol: water in a ratio of 7.5:1.5:1 (v/v). After the plates were developed, they were dipped into Vanillin sulfuric acid reagent and then heated at 105 °C for 5 min to visualize the spots corresponding to Shatavarin IV. The quantification of Shatavarin IV was performed by scanning the developed plates using a CAMAG TLC Scanner IV at a wavelength of 425 nm. Additionally, the peak purity of the isolated compound was verified by using the spectrum mode of the scanner to ensure accuracy.

**2.3. Combination Index Analysis.** CompuSyn software was employed to conduct the combination index (CI) analysis, aimed at evaluating the interaction between Shatavarin IV and Piracetam. The analysis focused on determining whether their combined use exhibited synergistic, additive, or antagonistic effects in the context of AD treatment. To achieve this, the dose-fixation method was applied, where the two compounds were combined at various fixed ratios to assess their effects


https://doi.org/10.1021/acsomega.4c09072
ACS Omega 2025, 10, 9132−9153

across different concentrations. The dose-fixation method involved preparing combinations of Shatavarin IV and Piracetam at fixed ratios. Starting with a 1:1 ratio, the combinations were tested sequentially at 1:2, 1:3, 1:4, and so on, up to a 1:9 ratio. By varying the ratios in this manner, we ensured that the full spectrum of possible interactions from low to high concentrations was covered. Using CompuSyn software, the data from the dose-fixation experiments were analyzed to calculate the CI values for each ratio. These values were then interpreted to identify whether the interaction between Shatavarin IV and Piracetam was synergistic (CI < 1), additive (CI = 1), or antagonistic (CI > 1). The software also facilitated the generation of dose−response curves and Fa-CI plots, which provided visual representations of the drug interactions at each ratio.[44]

**2.4. Optimization.** The optimization of the Shatavarin IV and Piracetam nanoemulsion formulation was carried out using the Box−Behnken design (BBD). Three critical factors were chosen for evaluation: oil concentration, surfactant concentration, and ultrasonication time, each examined at three different levels. The responses measured for the optimization process included the polydispersity index (PDI), particle size, and encapsulation efficiency (%EE), which were utilized to refine and enhance the formulation.

**2.5. Formulation of Nanoemulsion.** The preparation of the Shatavarin IV and Piracetam nanoemulsion was carried out by using the high-energy emulsification method. Initially, Shatavarin IV and Piracetam were dissolved in an appropriate oil phase, Capmul MCM C8, to form the oil phase, which served as the vehicle for the hydrophobic compounds. Meanwhile, the aqueous phase was prepared by mixing purified water with a surfactant such as Tween 80 and a cosurfactant Transcutol P. The choice of surfactant and cosurfactant was based on their ability to lower the interfacial tension between the oil and water phases, facilitating the formation of a stable emulsion. Once the oil phase and aqueous phase were prepared, they were mixed under high-speed homogenization to create a coarse emulsion. This pre-emulsified mixture was then subjected to ultrasonication, where high-frequency sound waves were applied to break down the droplets, reducing them to nanometer sizes. The ultrasonication process was continued for a specific duration, ensuring that the droplet size distribution was narrow, leading to a PDI that indicated uniformity of the droplet sizes.

**2.6. Characterization of Nanoemulsion.** *2.6.1. Dynamic Light Scattering.* To assess the physicochemical properties of the prepared nanoemulsion, advanced analytical techniques were employed. Malvern nano ZS Particle Sizing Systems, Inc. (UK) was utilized to determine the size and surface charge of the nanoemulsion using photon correlation spectroscopy (PCS) under an angle of 90° at a temperature of 25 °C. Particle size distribution (PDI) was also analyzed. Before measurement, samples were diluted in Milli-Q water.[45]

*2.6.2. Transmission Electron Microscopy.* The particle shape and surface morphology of the prepared nanoemulsion were examined using transmission electron microscopy (TEM) with the Tecnai G2 S-twin TEM instrument operating at 120 kV. The freshly prepared nanoemulsion sample was diluted at a 1:100 ratio using double-distilled water, followed by negative staining with 2% phosphotungstic acid. After being stained, the sample was air-dried on a copper grid. The images were captured and analyzed at 5000× magnification using Keen View FM and Olympus Soft Imaging Viewer software, respectively.[46]

*2.6.3. Differential Scanning Calorimetry.* The differential scanning calorimetry (DSC) procedure for analyzing the drug and its nanoformulation began with sample preparation. Approximately 2−5 mg of the pure drug (Piracetam or Shatavarin IV) was accurately weighed using an analytical balance and sealed in an aluminum DSC pan. The same procedure was followed for the lyophilized nanoemulsion formulation containing the drug with the help of 5% mannitol, ensuring a similar weight was used, and the sample was properly sealed in a separate pan. The DSC instrument was calibrated by using a standard material with a known melting point, such as indium or zinc, to ensure accurate temperature and enthalpy measurements. Once calibrated, the prepared DSC pans containing the drug sample and nanoemulsion formulation were placed in the sample chamber. An empty, sealed aluminum pan was used as a reference, as required by the instrument. The DSC scan parameters were set, typically covering a temperature range from 30 to 250 °C to include the melting points of the drug, excipients, and formulation components. The heating rate was set to 10 °C/min, with a nitrogen purge gas flow rate of 20−50 mL/min applied if necessary. The DSC analysis was then initiated, and the thermal behavior of both the pure drug and the nanoemulsion formulation was monitored, capturing thermograms that depicted any endothermic or exothermic peaks corresponding to phase transitions, melting points, or potential interactions.

*2.6.4. Fourier Transform Infrared.* PSNE and the pure Piracetam and Shatavarin IV were analyzed using Fourier transform infrared (FTIR) spectroscopy. Potassium bromide (KBr) powder was finely crushed with a tiny amount of pure Shatavarin IV and Piracetam in a 1:100 ratio, and the mixture was compacted into a pellet by using a hydraulic press. PSNE that had been lyophilized was similarly combined with KBr powder in the same proportion and compacted into a pellet. After that, a FTIR spectrometer was used to scan both KBr pellets across a 4000−400 $cm^{-1}$ range to identify distinctive functional groups and find any possible interactions between the medications and the nanoemulsions constituent parts.

**2.7. Antioxidant Assay.** The antioxidant capacity of PSNE was assessed by using the 2,2-diphenyl-1-picrylhydrazyl (DPPH) method. The ability of a chemical to act as an antioxidant can be assessed by using the DPPH free radical technique. The violet color of the DPPH solution turns colorless at room temperature due to the antioxidants' capacity to transfer electrons. Before the DPPH methanolic solution was used, the sample (0.5 mL) was dissolved in 3 mL of methanol (0.3 mL). The reaction mixture was kept in a dark area for 1 h to complete the reaction process. Due to the sample's ability to donate hydrogen, the color change reflects its antioxidant capacity. The blank contained 3.3 mL of methanol and 0.3 mL of sample, whereas the control contained 3.5 mL of methanol and DPPH solution (0.3 mL). Spectrophotometry was employed to analyze the substance at 517 nm.[47]

**2.8. Entrapment Efficiency of Nanoemulsion.** Using the ultracentrifugation-filtration method, the EE % of prepared PSNE was assessed. To remove the big aggregates, the formulation was first filtered. The filtered nanoemulsion was then centrifuged using a Beckman Coulter LE 80 ultra-centrifuge at 25,000*g* for 45 min, keeping the temperature between 0 and 4 °C. The supernatant containing Piracetam


https://doi.org/10.1021/acsomega.4c09072
ACS Omega 2025, 10, 9132−9153

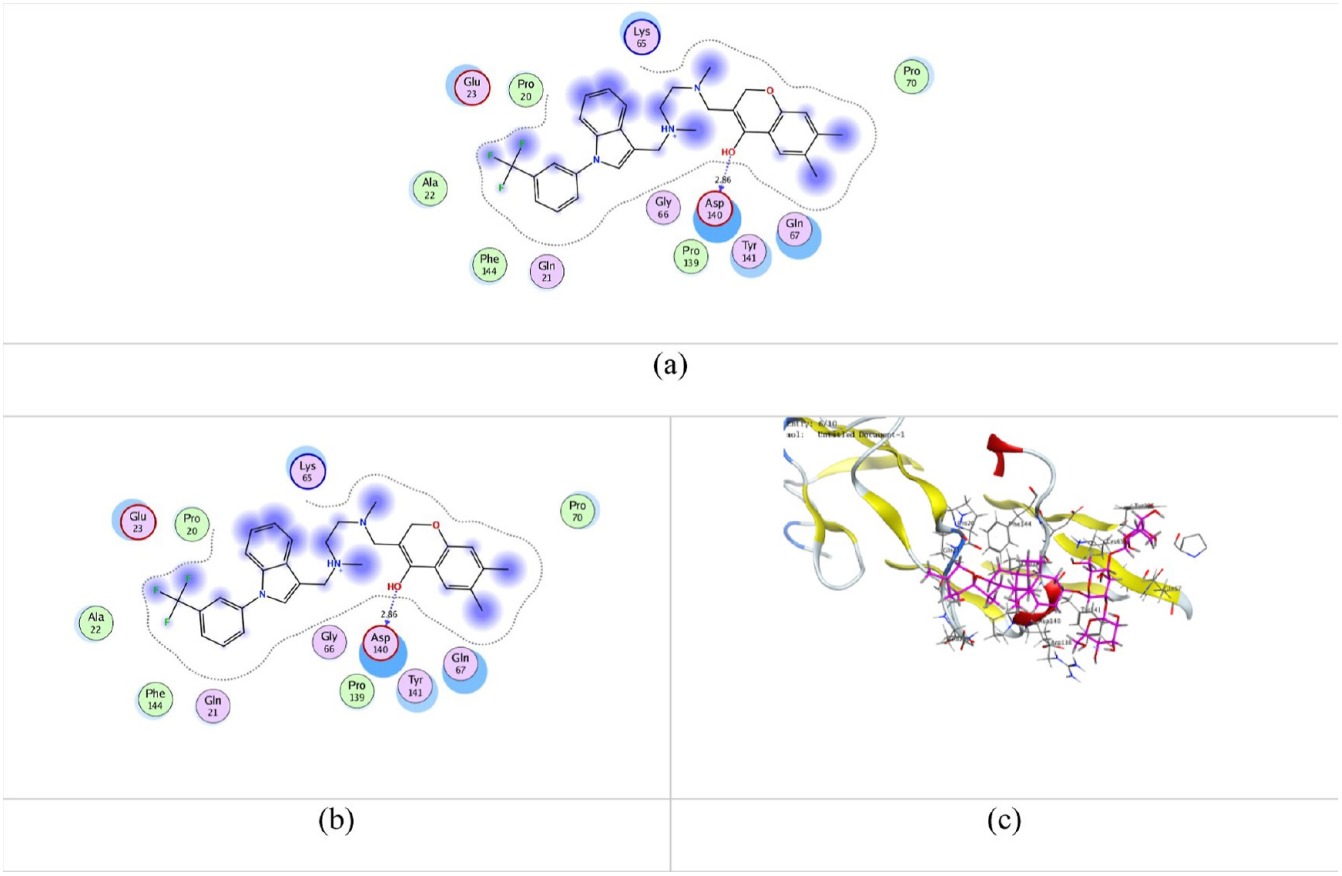


**Figure 1.** Molecular docking analysis with TNF-$\alpha$ (PDB ID: 2AZ5) of (a) internal ligand; (b) Shatavarin IV 2D; and (c) Shatavari IV 3D.

and nonencapsulated Shatavarin IV was carefully separated after centrifugation. A Shimadzu UV-1601 spectrophotometer (Shimadzu Corp., Kyoto, Japan) was used to determine the quantity of unencapsulated Shatavarin IV and Piracetam present in the supernatant following the proper dilution with methanol to ensure precise quantification.[48]

**2.9. *In Vitro* Release Study.** For the *in vitro* drug release study of piracetam, the dialysis bag method was employed. A nanoemulsion containing 1 mg/mL of Piracetam was placed in a presoaked dialysis bag with a molecular weight cutoff of 12−14 kDa. The bag was immersed in 100 mL of PBS (pH 7.4) at 37 °C with constant stirring at 100 rpm using a magnetic stirrer. At predetermined time points, aliquots of the release medium were collected and replaced with an equal volume of fresh PBS to maintain the sink conditions. The collected samples were analyzed spectrophotometrically (UV-1601, Shimadzu Corp., Kyoto, Japan) at a wavelength of 214 nm to quantify the amount of Piracetam released. The cumulative drug release (CDR) was calculated and plotted over time to evaluate the release profile of Piracetam from the nanoemulsion. The experiment was conducted in triplicate to ensure accuracy and reproducibility, and the results were analyzed using various kinetic models to assess drug release behavior.[49]

**2.10. Ex Vivo Permeation Study.** The experiments were conducted using a noneverted gut sac model. Rats were fasted overnight with access to water only and were euthanized using anesthetic ether just before the procedure. The intestines were surgically excised and rinsed with saline, and a 5 cm section of the ileum was isolated. For the experimental group, PSNE and suspension were dissolved in 1 mL of water and introduced into the mucosal side of the intestinal sacs, which were then securely ligated at both ends. Each sac was submerged in a jacketed glass assembly containing 100 mL of Krebs solution, prewarmed to 37 °C. The temperature was maintained by circulating hot water through the jacket, and the Krebs solution was continuously oxygenated with a 95% O2 supply for a total of 120 min. Drug transport was assessed by collecting samples from the serosal medium at specific intervals throughout the 120 min. After each 2 mL sample was taken from the serosal medium, it was replenished with fresh Krebs solution. The withdrawn samples were analyzed spectrophotometrically (UV-1601, Shimadzu Corp, Kyoto, Japan) at a wavelength of 214 nm to measure the amount of permeated Piracetam.[50−52]

**2.11. MTT Assay.** A cytotoxicity assessment was conducted using the EZcount MTT Cell Assay kit (HiMedia, India) protocol to determine the cell viability of a drug sample. In the laboratory procedures for thawing Neuron (N2a) cells, the cells were transferred from −80 °C or liquid nitrogen storage to room temperature, followed by a brief incubation at 37 °C for 1 min. The thawed cells were transferred to a biosafety hood and gradually added to a 50 mL falcon tube containing 2 mL of Dulbecco's Modified Eagle Medium (DMEM), followed by the addition of 3 mL of more of the media. After centrifugation at 1500 rpm for 10 min, the supernatant was removed, and the cell pellet was resuspended in 5 mL of DMEM. The suspension was then transferred to a T-25 $cm^2$ culture flask, and cell viability was confirmed by microscopic observation before incubating at 37 °C with 5% $CO_2$. For cell splitting, N2a cells at 90% confluence had the supernatant



https://doi.org/10.1021/acsomega.4c09072
ACS Omega 2025, 10, 9132−9153

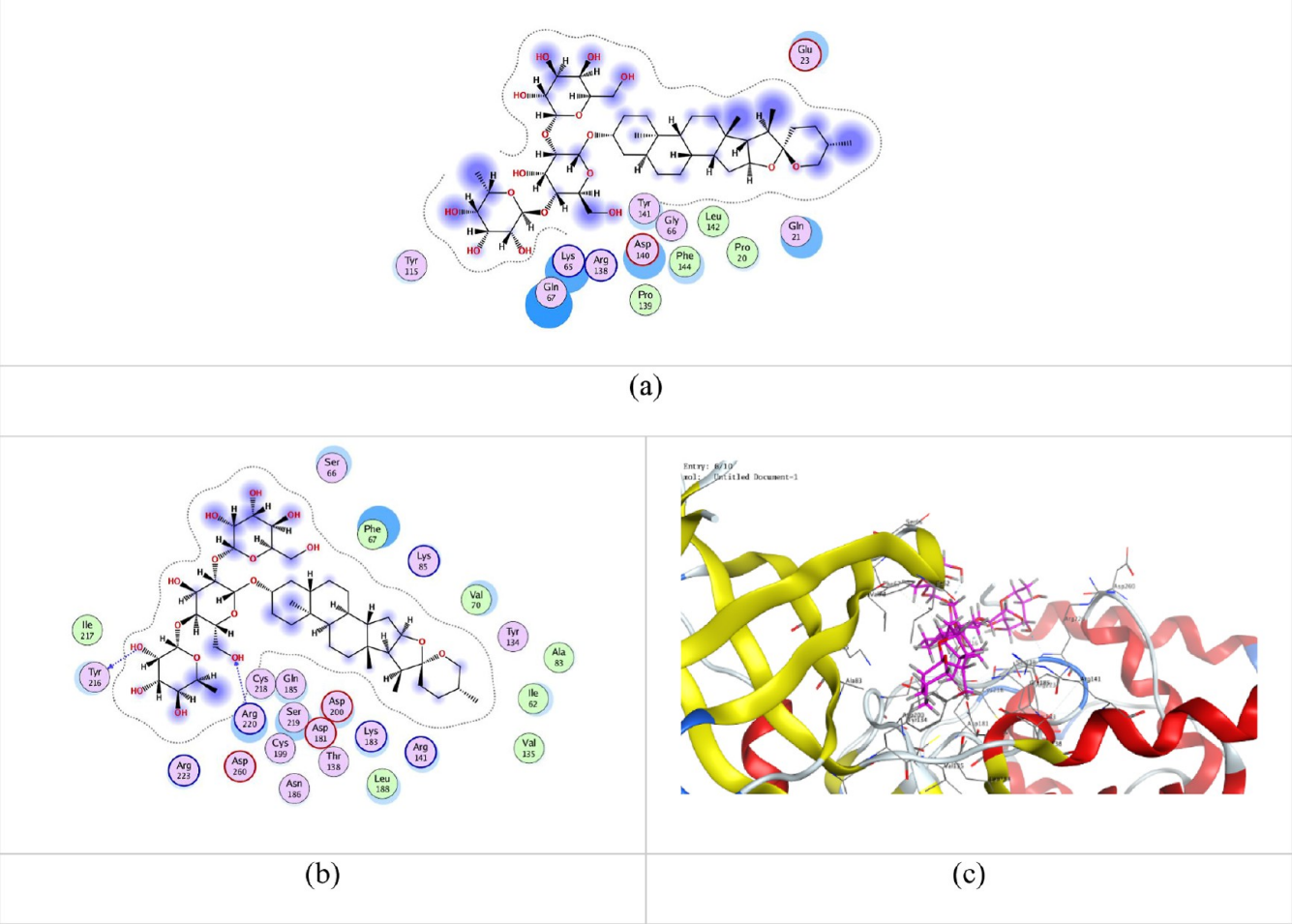


**Figure 2.** Molecular docking analysis with Gsk3 axin complex (PDB ID: 4NM0) of (a) internal ligand; (b) Shatavarin IV 2D; and (c) Shatavarin IV 3D.

removed, followed by detachment using 1% trypsin−EDTA. The detached cells were resuspended in DMEM, with 2 mL transferred to a new flask, and fresh media added to both flasks. The flasks were incubated at 37 °C and checked the next day for successful cell attachment. In the cytotoxicity assay, N2a cells were seeded into a 96-well plate. A stock solution of the PSNE (2 mg/mL) was prepared in DMEM. Cells were treated with varying concentrations of the nanoemulsion (1 to 1000 $\mu$g/mL) for 24 h. Afterward, the media was replaced with phenol red-free DMEM, MTT reagent was added, and the plate was incubated for 3 h. Absorbance was measured at 570 nm using an ELISA reader, with all measurements conducted in triplicate to calculate percentage cell viability.[44]

**2.12. pH Measurements and Conductivity.** The pH of the prepared samples was measured using a handheld pH meter. The pH of the nanoemulsions was recorded immediately after immersing the pH meter's probe directly into the sample. The measurements were conducted at a temperature of 25 °C. Additionally, the same device was used to measure the electrical conductivity of the nanoemulsions at the same temperature.[53]

**2.13. Physical Stability Tests.** Throughout six months, the samples were kept in sealed microcentrifuge tubes (MCTs) at varied temperatures. Three different temperatures were used for storage: 25 °C with 60% relative humidity (RH), 40 °C with 75% RH, and 5 °C. The samples' conductivity, pH, zeta potential, particle size, and PDI were measured at various points during the storage period. To guarantee accuracy, each measurement was carried out three times.[54]

**2.14. Statistical Analysis.** The statistical analysis was performed using GraphPad Prism software with the results expressed as the mean ± standard deviation (SD). For the statistical evaluation of the BBD, analysis of variance (ANOVA) was employed.

## 3. RESULTS AND DISCUSSION

**3.1. *In Silico* Study.** The molecular docking study confirmed the selectivity and potency of Shatavarin IV in binding to various AD-related targets.

*3.1.1. In Silico Binding Capacity of Shatavarin IV to TNF-α (PDB ID: 2AZ5).* The molecular docking analysis of Shatavarin IV with TNF-$\alpha$ revealed a binding affinity of −7.29 kcal/mol, which was stronger than the internal ligand's binding affinity of −6.2248 kcal/mol. Interaction analysis of all possible docked conformers of Shatavarin IV showed favorable interactions within the 2AZ5 binding pocket (Figure 1).

*3.1.2. In Silico Binding Capacity of Shatavarin IV to GSK-3 Axin Complex (PDB ID: 4NM0).* Shatavarin IV exhibited a strong binding affinity of −9.6785 kcal/mol, which was significantly higher than the internal ligand's affinity of −6.9775 kcal/mol. The interaction analysis revealed robust binding within the 4NM0 binding site (Figure 2).



https://doi.org/10.1021/acsomega.4c09072
ACS Omega 2025, 10, 9132−9153

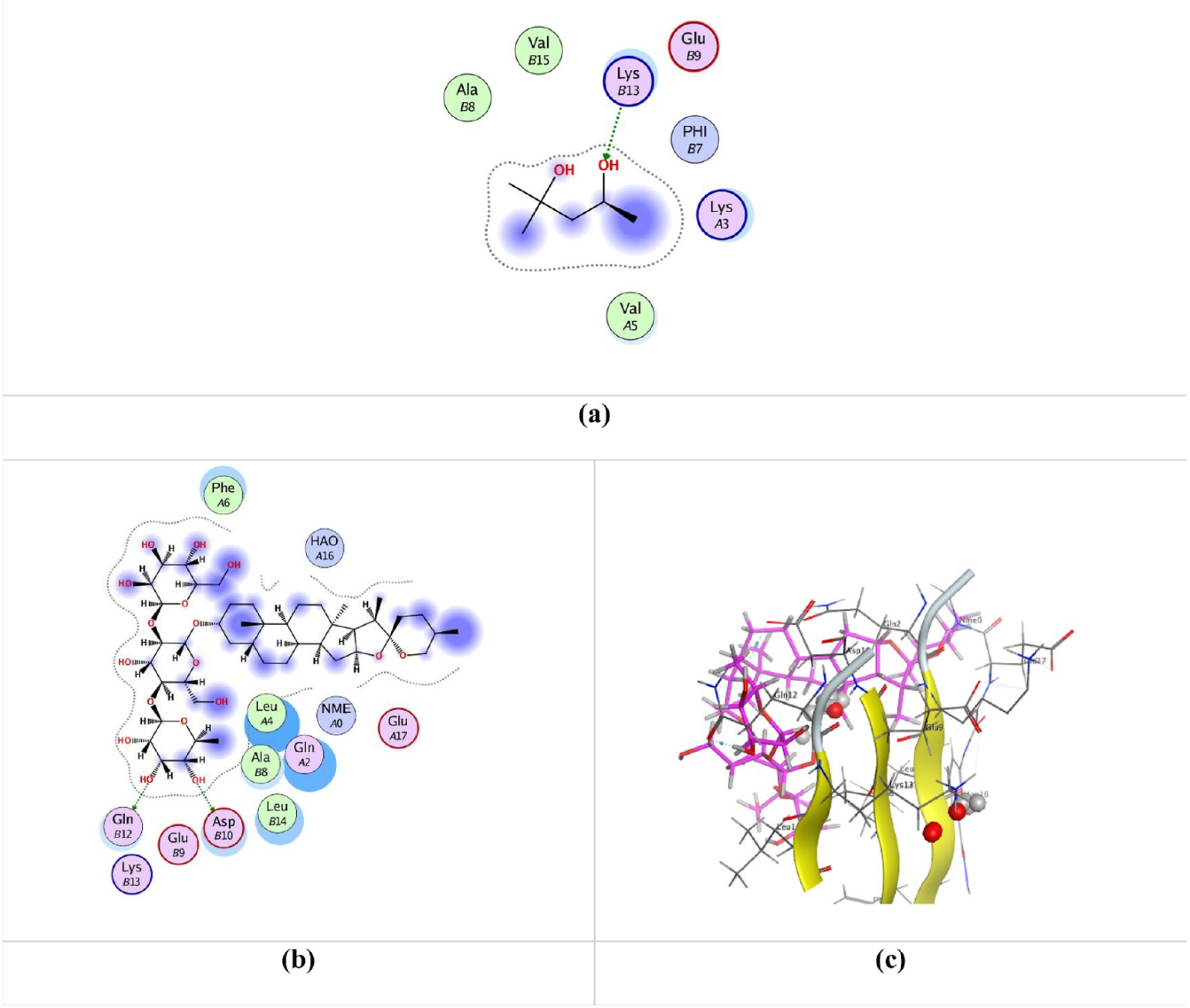


**Figure 3.** Molecular docking analysis with amyloid-$\beta$ (PDB ID: 4Q8D) of (a) internal ligand; (b) Shatavarin IV 2D; and (c) Shatavarin IV 3D.

*3.1.3. In Silico Binding Capacity of Shatavarin IV to Amyloid-$\beta$ (PDB ID: 4Q8D).* The docking analysis of Shatavarin IV with A$\beta$ presented a binding affinity of −6.8326 kcal/mol, which was more favorable than the internal ligand's affinity of −4.0537 kcal/mol. Interaction analysis demonstrated the formation of key interactions within the 4Q8D binding pocket (Figure 3).

*3.1.4. In Silico Binding Capacity of Shatavarin IV to GSK-3 $\beta$ Complex (PDB ID: 1H8F).* Shatavarin IV showed a strong binding affinity of −8.8243 kcal/mol compared to the internal ligand's affinity of −6.1783 kcal/mol. Interaction analysis of docked conformers highlighted significant interactions within the 1H8F binding site (Figure 4).

**3.2. Extractions and Analytical Methods.** The extraction process resulted in the isolation of 401.1 2.3 mg of Shatavarin IV from 250 g of root powder, with a purity of 66%, as confirmed by HPTLC. The physical characteristics of the isolated compound included a beige-colored shiny powder with a melting point of 250−255 °C. As depicted in Table 1, the compound exhibited solubility in both b and methanol, and the purity was validated through HPTLC with a peak at 0.45 ± 0.05 Rf. Fractionation by column chromatography with a mobile phase of ethyl acetate: methanol: water (8:1:1 v/v) followed by TLC analysis identified fractions 10 to 22 exhibiting $R_f$ values similar to those of the Shatavarin IV standard (Figures 5 and 6).

The isolated compound's physical characteristics were consistent with those of Shatavarin IV (Table 1). The optimized isolation technique produced Shatavarin IV with a purity of 66%, as confirmed through a comparison to a reference standard via HPTLC (Figure 7). Peak purity was further validated with spectral detection at an $R_f$ value of 0.45 ± 0.05 (Figure 8). Specifically, this method yielded 401.1 ± 2.3 mg of Shatavarin IV from 250 g of root powder, outperforming the yields obtained from alternative isolation techniques.

There were significant variations in purity levels based on temperature conditions during column chromatography. At a cold atmospheric temperature (17−22 °C), the highest purity of 66% was achieved, while isolations performed at standard room temperature (22−27 °C) resulted in a slightly lower purity of 56%. At an elevated temperature (27−32 °C), the


https://doi.org/10.1021/acsomega.4c09072
ACS Omega 2025, 10, 9132−9153

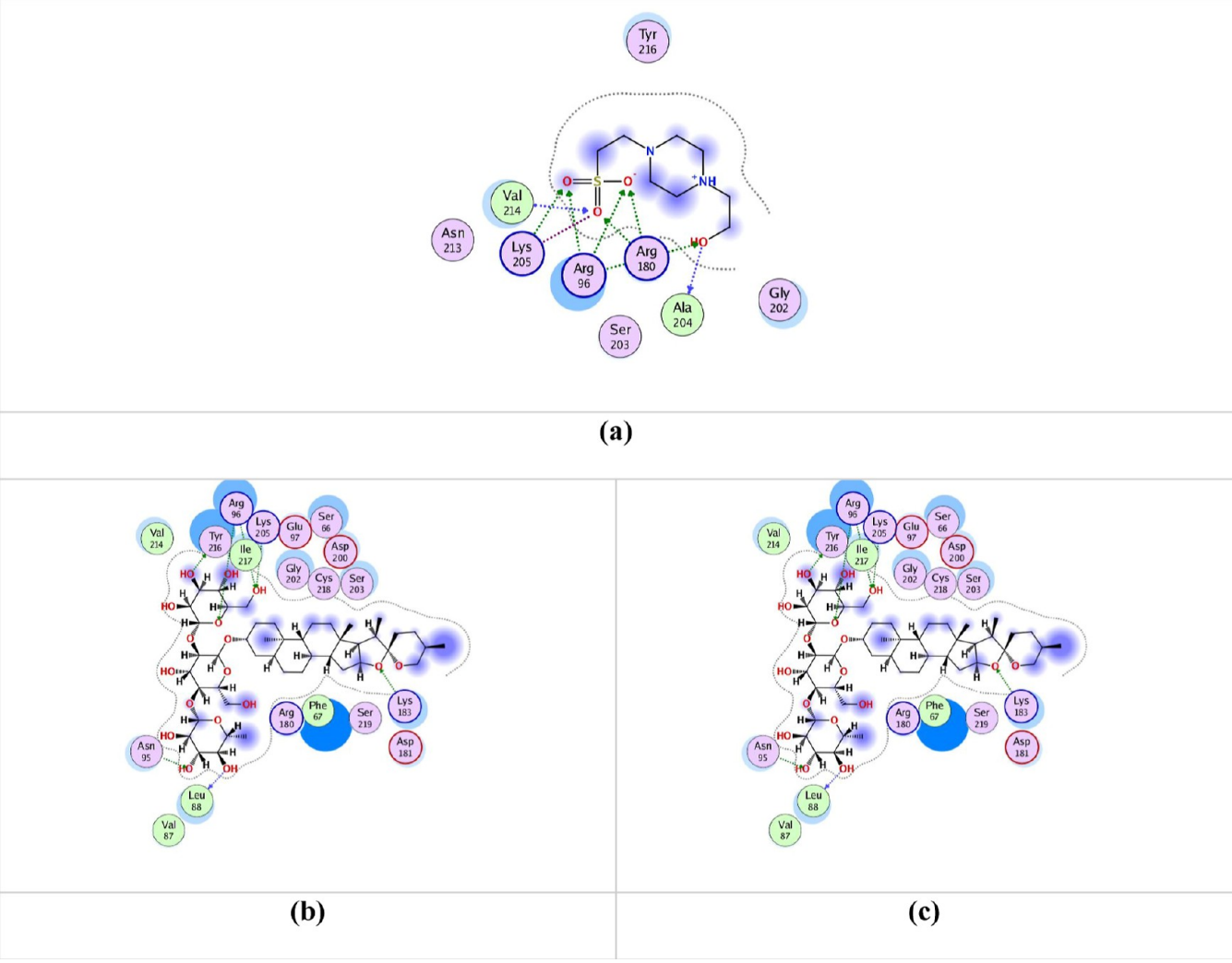


**Figure 4.** Molecular docking analysis with GSK-3 beta (PDB ID: 1H8F) of (a) internal ligand; (b) Shatavarin IV 2D; and (c) Shatavarin IV 3D.

**Table 1. Physical Characteristics of the Isolated Compound**

| parameters | characteristics |
|---|---|
| Color | Beige color shiny powder |
| State | Solid |
| Solubility | Water and Methanol |
| Melting point | 250−255 °C 7 |
| Yield | 401.1 ± 2.3 mg from 250 g crude drug |
| Purity (%) | 66% |

purity significantly declined to 37%, likely due to the decomposition of certain compounds or the volatilization of specific constituents from the crude extracts. HPLC fingerprinting analysis of *A. racemosus* root extract was conducted using a solvent system of ethyl acetate: methanol: formic acid (7.5:1.5:1 v/v), which developed the TLC plate. Densitometry scanning at 254, 366, and 540 nm revealed metabolites at distinct $R_f$ values. At 254 nm, major and minor metabolites were detected at $R_f$ values of 0.01, 0.69, and 0.82; at 366 nm, metabolites were observed at $R_f$ values of 0.01, 0.09, 0.69, and 0.81; and at 540 nm (after derivatization with anisaldehyde reagent), metabolites appeared at $R_f$ values of 0.01, 0.04, 0.12, 0.15, 0.68, and 0.82. The extractive values of the samples showed significant variation, indicating substantial differences within the samples themselves. The percentage yield of the methanolic extract was calculated to be 23.653%, which falls within the established limits outlined in the Ayurvedic Pharmacopoeia of India. This study also identified a wide range of metabolites present in *A. racemosus* samples. During method validation, the developed protocol demonstrated linearity, robustness, and precision across a range of concentrations (1, 2, 5, 10, and 25 $\mu$L/mL). The calibration equation was determined to be $71.507x + 1976.916$, with a regression coefficient ($r^2$) of 0.98842, indicating strong linearity. Quantitative analysis revealed Shatavarin IV as a key metabolite, accounting for 0.121% of the total extract, indicating its prominence in *A. racemosus*.

**3.3. Combination Index Analysis.** The CompuSyn program was employed to automatically calculate the CI equation (CIE), which identifies synergism (CI < 1), additive effects (CI = 1), and antagonism (CI > 1). The $IC_{50}$ value for the CI was determined to be 187.5 $\mu$g/mL at a 1:1 ratio of Piracetam and Shatavarin IV (test and standard drugs). This ratio resulted in the highest cell viability within 24 h. The CI for this ratio, calculated using CompuSyn 1.0, was found to be 0.10843, indicating a strong synergistic effect (Figure 9).

**3.4. Optimization of PSNE.** Figure 10 graphs are based on a linear model, as indicated by the $R^2$ values for each response, which showed a high degree of fit between the predicted and


https://doi.org/10.1021/acsomega.4c09072
ACS Omega 2025, 10, 9132−9153

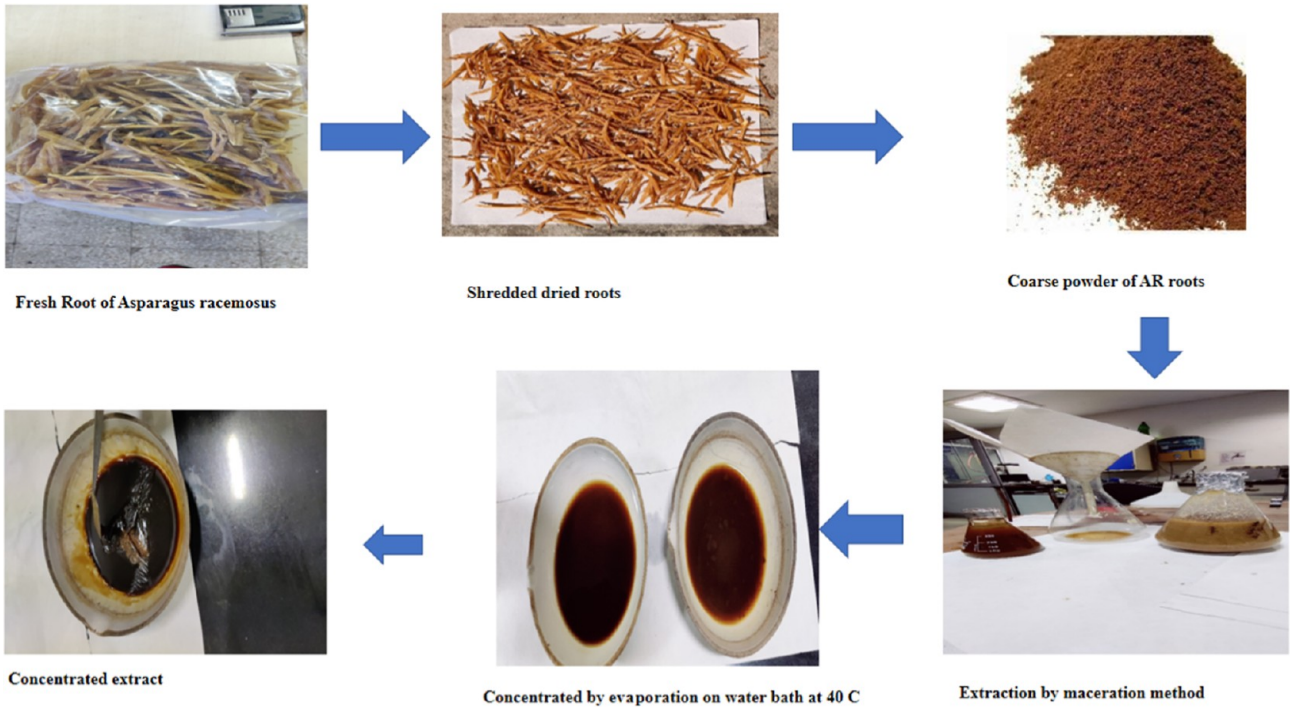


**Figure 5.** Flowchart of the extraction process of *A. racemosus* tuberous roots for methanolic extract.

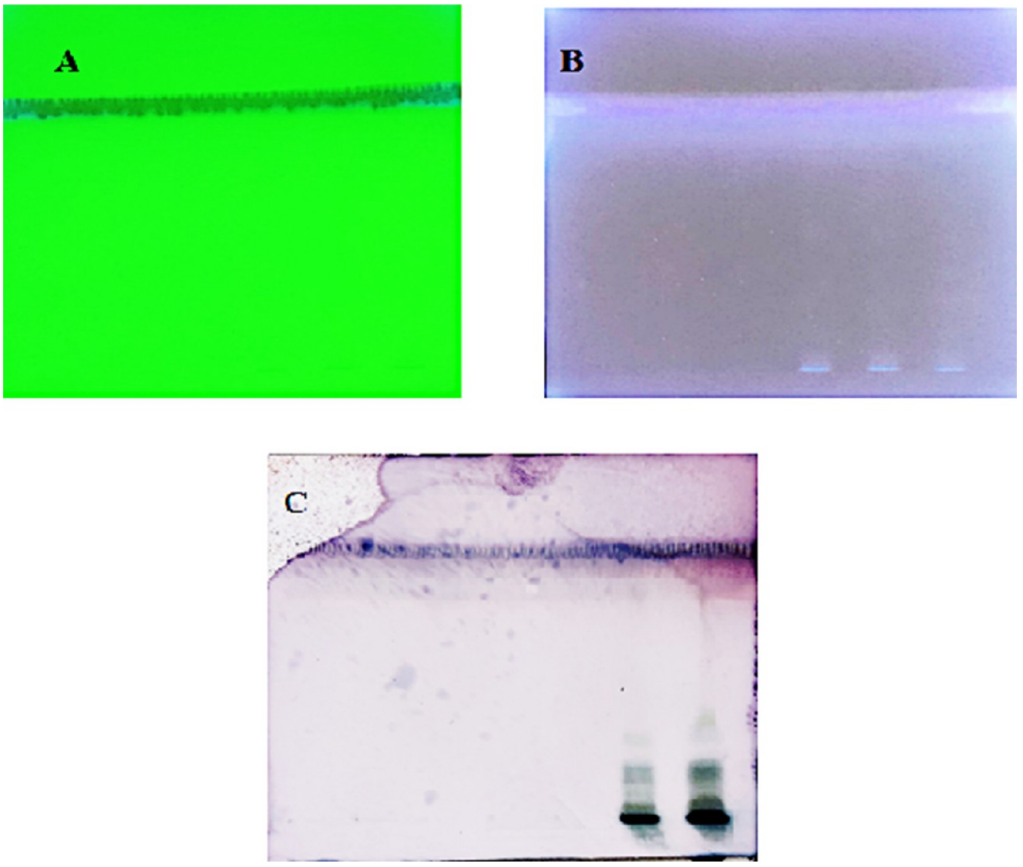


**Figure 6.** HPTLC at (A) 254 nm, (B) 366 nm, and (C) 540 nm after derivatization (solvent system ethyl acetate: methanol: formic acid (7.5:2:0.5 v/v).

observed data points, reflecting the robustness of the model in describing the relationships among the variables (Tables 3, 4, and 5). For particle size, the model demonstrated an $R^2$ value of 0.9582, an adjusted $R^2$ value of 0.9467, and a predicted $R^2$ value of 0.9119. This indicated that the model explains 95.82% of the variability in particle size due to changes in oil and $S_{mix}$



https://doi.org/10.1021/acsomega.4c09072
ACS Omega 2025, 10, 9132−9153

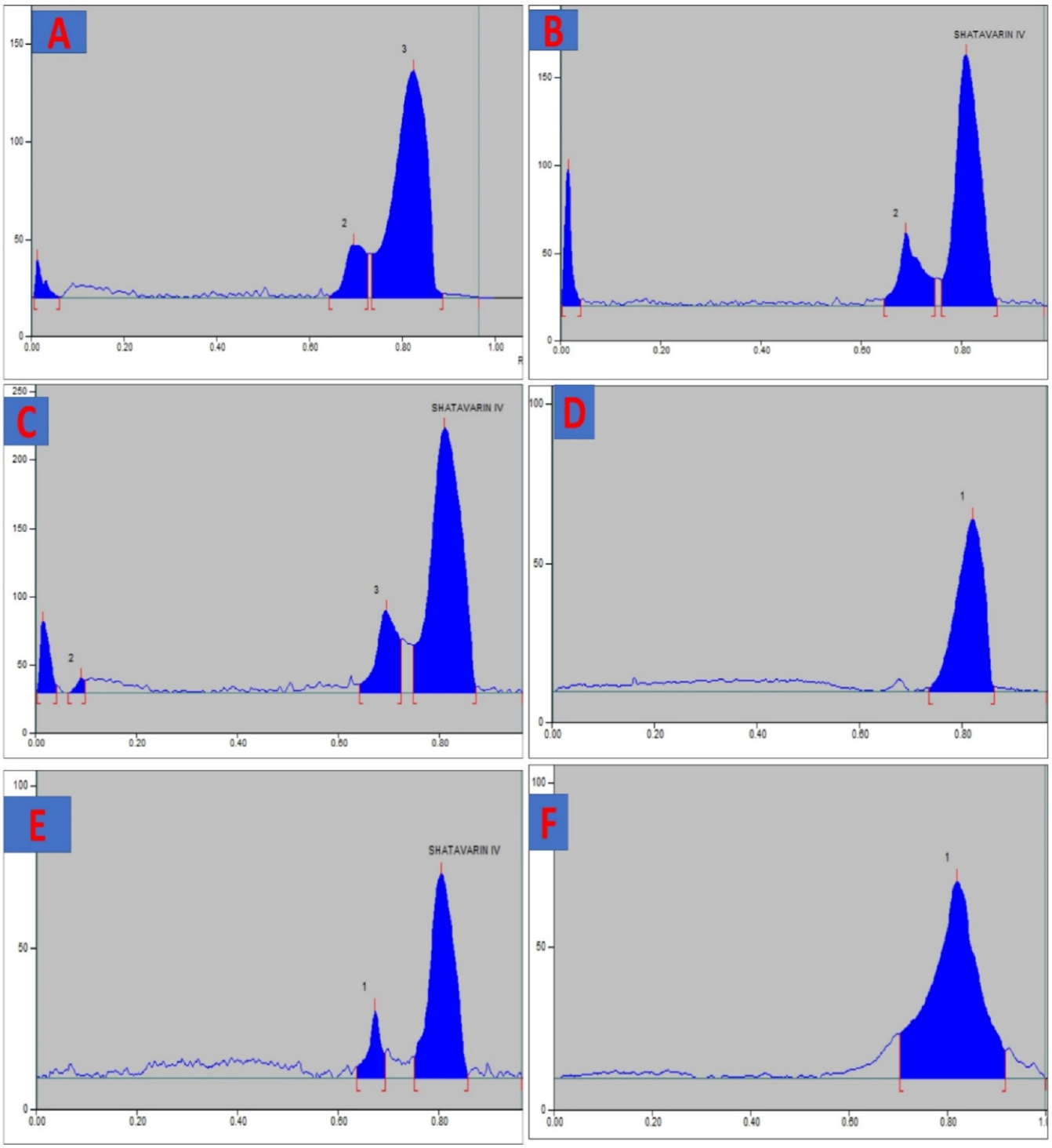


**Figure 7.** HPTLC chromatogram of (A) methanolic extract of *Asparagus racemosus* at 254 nm, (B) methanolic extract of *A. racemosus* at 366 nm, (C) methanolic extract of *A. racemosus* at 540 nm, (D) standard Shatavarin IV at 254 nm, (E) standard Shatavarin IV at 366 nm, and (F) standard Shatavarin IV at 540 nm.

percentages, with the adjusted $R^2$ and predicted $R^2$ suggesting that the model retains its predictive accuracy after adjustment for the number of predictors. The relatively high $R^2$ values confirm that the linear model effectively captures the influence of the two variables on the particle size. Based on the data presented, the individual desirability values were calculated as follows: 0.95 for particle size, 0.90 for PDI, and 0.98 for EE. The combined desirability value for all factors was 0.94, indicating a high level of optimization (Table 2).

Graph A depicts the interaction between oil percentage and $S_{mix}$ percentage on particle size, where increasing the oil percentage results in a slight decrease in particle size, suggesting that oil may act to break down particles or reduce aggregation, possibly due to its role in modulating the viscosity or stabilizing the system. Conversely, higher $S_{mix}$ percentages led to larger particle sizes, which could be attributed to the increased surfactant-*co*-surfactant concentration altering the droplet size during emulsification or aggregation processes.



https://doi.org/10.1021/acsomega.4c09072
*ACS Omega* 2025, 10, 9132−9153

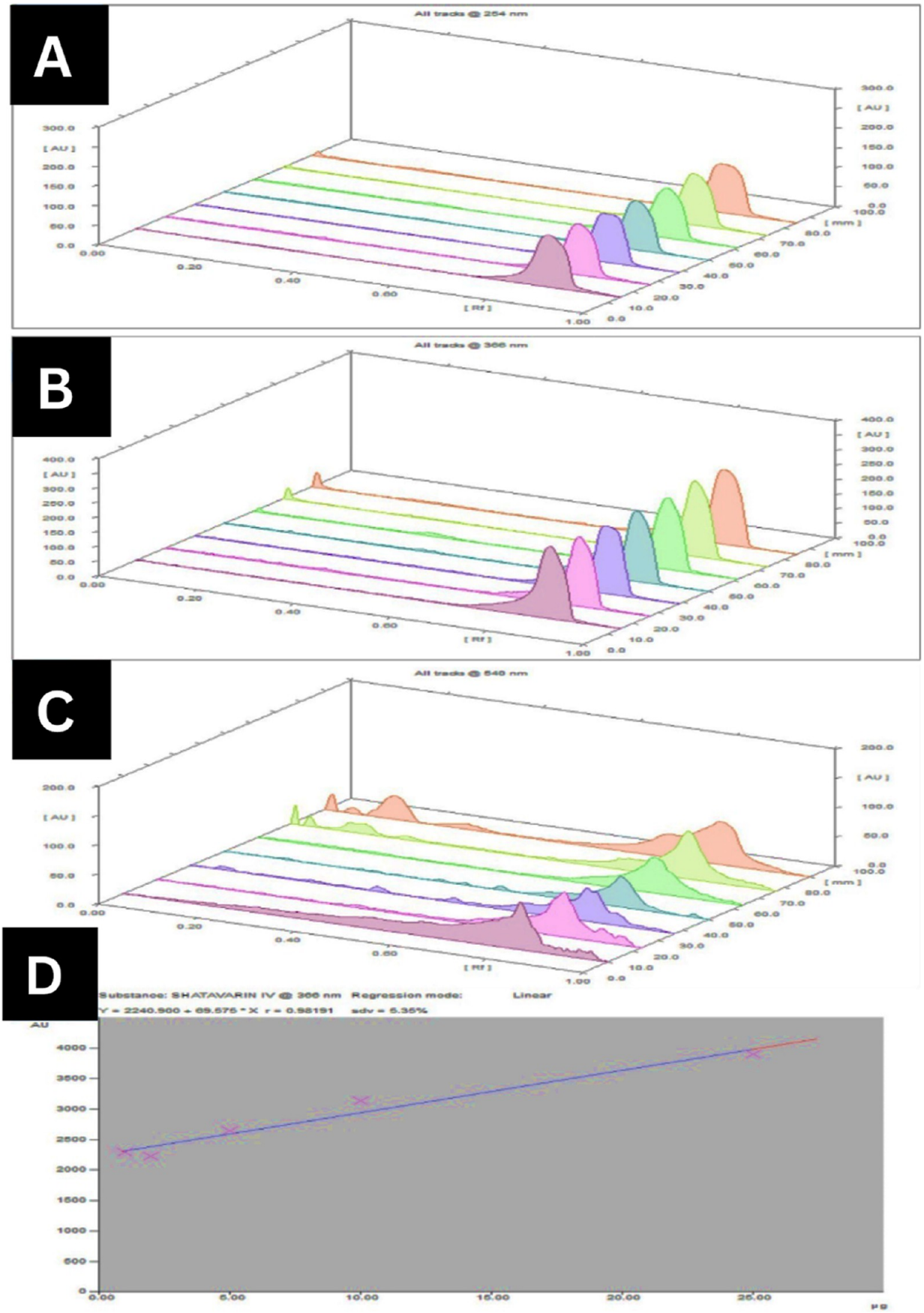


**Figure 8.** HPTLC chromatogram of (A) 3D overlay of standard and sample of *A. racemosus* extract at 254 nm, (B) 3D overlay of standard and sample of *A. racemosus* extract at 366 nm, (C) 3D overlay of standard and sample of *A. racemosus* extract at 540 nm, and (D) calibration curve of Shatavarin IV.



https://doi.org/10.1021/acsomega.4c09072
*ACS Omega* 2025, 10, 9132−9153

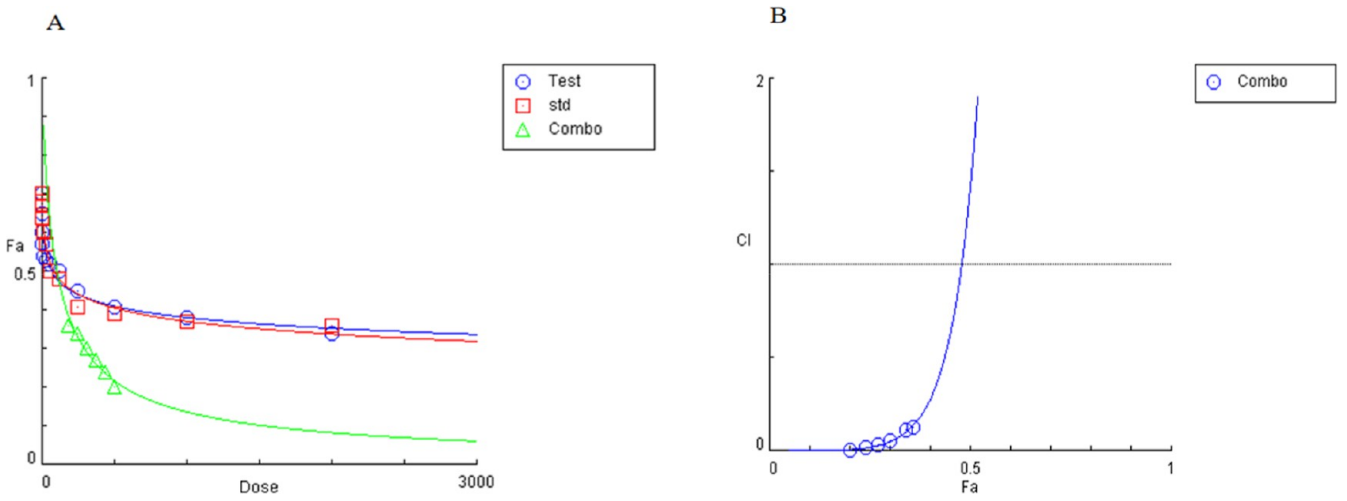


**Figure 9.** (A) Dose−effect curve: combo (test + Std [1:1]) and (B) combination index plot.

This suggested that a nuanced balance is required to achieve the optimal particle size by adjusting these two variables. Graph B illustrates that a longer sonication time significantly reduces particle size, a direct result of prolonged mechanical energy input, breaking down larger particles into smaller ones. This effect is seen across all levels of oil percentage, which continues to show a slight reduction in particle size, indicating that the mechanical process of sonication is a dominant factor in controlling the particle size, regardless of the oil content.

For PDI, the $R^2$ value is 0.9540, the adjusted $R^2$ value is 0.9414, and the predicted $R^2$ value is 0.9033. These values suggest that 95.4% of the variability in PDI is explained by the model, and the close alignment between adjusted and predicted $R^2$ values further reinforces the model's robustness and suitability for predicting PDI based on the given variables. The slightly lower predicted $R^2$ compared to the adjusted $R^2$ indicates a minor degree of overfitting; however, the model is still reliable in capturing the essential trends and patterns associated with the formulation variables. Graph C focuses on PDI, demonstrating that a more uniform PDI (indicated by lower PDI values) is achieved at lower oil and $S_{mix}$ percentages. As either variable increases, PDI also increases, suggesting that higher concentrations may cause broader PDIs, potentially due to the formation of aggregates or variable droplet sizes during the formulation process. This pattern is further supported by graph D, which showed that increasing sonication time led to a substantial decrease in PDI, highlighting the role of sonication in creating a more homogeneous particle distribution by effectively breaking down larger particles or aggregates into smaller, uniformly sized particles. Conversely, increasing the oil percentage has a lesser but noticeable impact on increasing PDI, which could be due to the variability introduced in the system by a higher oil content.

For EE %, the model shows exceptionally high $R^2$ values: an $R^2$ of 0.9940, an adjusted $R^2$ of 0.9924, and a predicted $R^2$ of 0.9905. These values indicated that the model accounts for 99.4% of the variability in EE, with minimal difference between the adjusted and predicted $R^2$ values. This reflected a highly accurate and reliable model fit, suggesting that the linear model is exceptionally effective in predicting the relationship between oil and $S_{mix}$ percentages and the EE. The small gap between the adjusted and predicted $R^2$ values further confirms that the model is not overfit and remains highly predictive. Graph E shows that EE % is significantly enhanced with higher $S_{mix}$ percentages, likely due to the better stabilization of the formulation and more effective interaction between the active ingredient and the surfactant mixture, which facilitates better encapsulation. However, increasing the oil percentage slightly decreased the EE %, possibly due to the dilution of the surfactant's effect or reduced interactions necessary for effective encapsulation. Graph F shows that longer sonication times led to higher EEs. This is likely because prolonged sonication helps in uniformly dispersing the active ingredient within the formulation, preventing aggregation, and ensuring that more of the active ingredient is retained within the encapsulated particles. However, even with increased sonication time, a higher oil percentage shows a slight reduction in EE %, suggesting that an optimal balance of the oil content is necessary to achieve maximum EE. To achieve the desired particle characteristics, such as smaller particle sizes, a uniform particle distribution, and higher EE, the formulation should ideally utilize lower oil percentages combined with higher $S_{mix}$ concentrations and longer sonication times. This balance ensures efficient emulsification, stabilization, and active ingredient retention, ultimately enhancing the formulation's effectiveness and performance for its intended application.

**3.5. Characterization.** *3.5.1. Particle Size and PDI.* The average particle size (Z-average) was 183.6 nm. The PDI of the sample is 0.194, which indicates a relatively narrow size distribution (Figure 11). A PDI value below 0.2 suggests that the particles are fairly uniform in size, reflecting a monodisperse or homogeneous distribution. The analysis also shows a single prominent peak at 214.5 nm, which accounts for 100% of the intensity, confirming that the majority of the particles are concentrated around this size. The standard deviation for this peak is 84.01 nm, indicating some degree of variability around the mean size, although still within acceptable limits for uniformity.

*3.5.2. Transmission Electron Microscopy.* The TEM of the nanoemulsion formulation shows spherical particles with sizes ranging from approximately 189.12 to 215.27 nm (Figure 12). The particles appear well-dispersed with a relatively uniform size distribution, which is consistent with a monodisperse system. The spherical shape and smooth surface morphology indicate that the nanoemulsion droplets are well-formed, suggesting successful formulation with minimal aggregation or


https://doi.org/10.1021/acsomega.4c09072
ACS Omega 2025, 10, 9132−9153

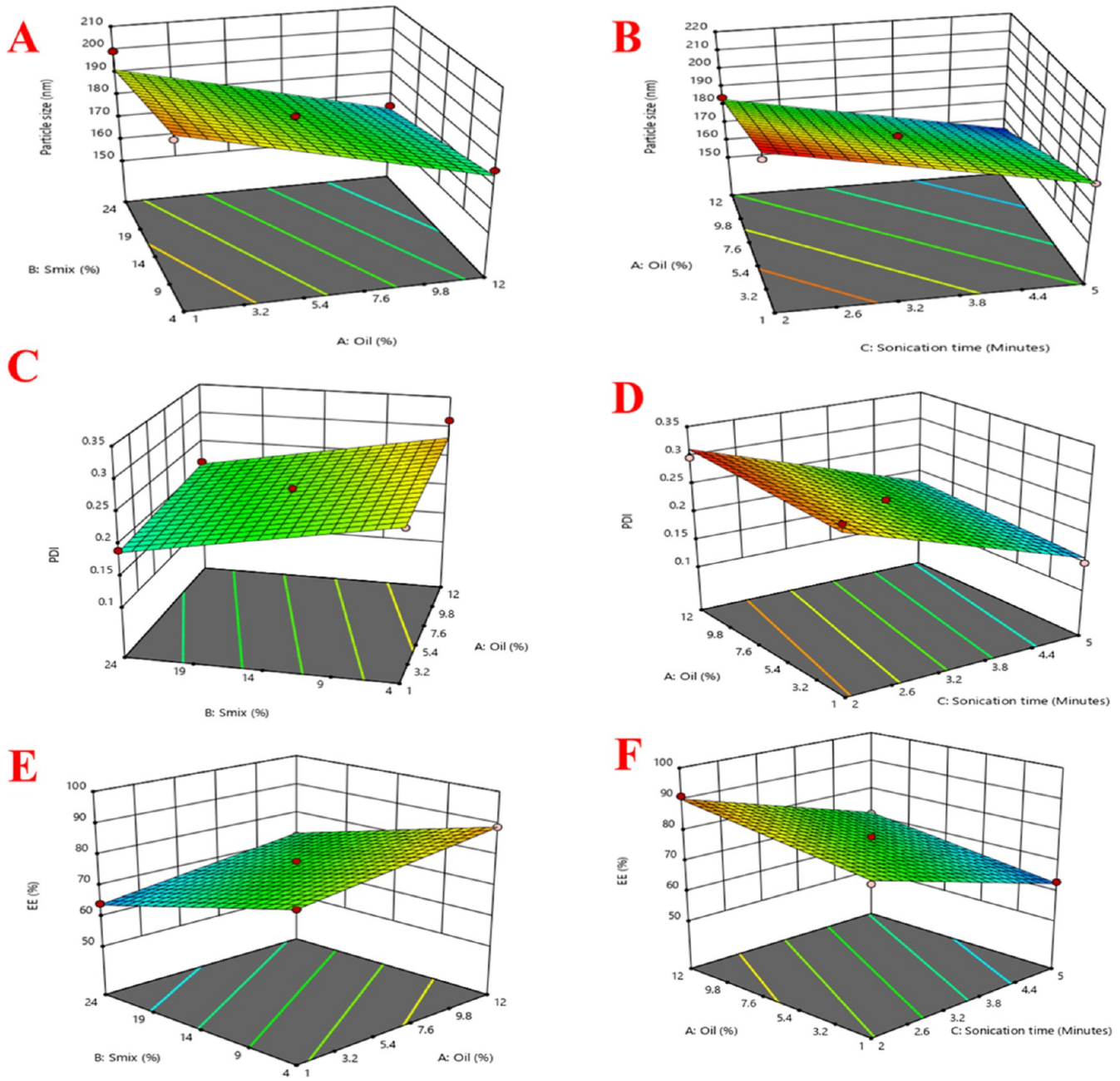


**Figure 10.** 3D surface graphs generated by design expert software provide an in-depth visualization of how varying the formulation components—oil percentage (A), $S_{mix}$ percentage (B), and sonication time (C)—influence critical response variables: (A,B) particle size (nm), (C,D) PDI, and (E,F) EE %.

fusion. The scale bar of 200 nm further confirms that the observed particles fall within the expected nanometer range, consistent with nanoemulsion characteristics. The particle sizes observed in this TEM image align well with the DLS data from the previous report, which showed a *Z*-average of 183.6 nm, supporting the reliability and consistency of the particle size analysis across different measurement techniques. Overall, this TEM micrograph validates the uniformity and nanoscale size of the particles in the optimized nanoemulsion, which is essential for applications where consistent PDI is critical, such as drug delivery or targeted therapies.

*3.5.3. Differential Scanning Calorimetry.* The DSC analysis revealed distinct endothermic peaks for the individual components and nanoemulsion formulation. As depicted in Figure 13, Piracetam exhibited an endothermic peak at 175.13 °C, corresponding to its melting point, while Shatavarin IV shows a separate endothermic peak at 216.59 °C, indicative of its crystalline nature. In contrast, the DSC thermogram of the PSNE formulation displays a single endothermic peak at 147.42 °C and a pure mannitol peak at 158.22 °C, a common excipient present in the formulation, but there was shifting in the peak. The shift in the DSC peak of mannitol from 158.22 °C in its pure form to 147.42 °C in the nanoemulsion formulation does not adversely affect the stability or functionality of the nanoemulsion. Instead, this phenomenon highlights beneficial aspects, such as enhanced interaction of mannitol with surfactants, cosurfactants, or oils, which contribute to improved solubility and dispersion in the


https://doi.org/10.1021/acsomega.4c09072
ACS Omega 2025, 10, 9132−9153

**Table 2. Runs for Optimization of Formulation and Responses**

| Standard | Run | Factor 1 A: Oil (%) | Factor 2 B: $S_{mix}$ (%) | Factor 3 C: Sonication Time | Response 1 Particle size (nm) | Response 2 PDI | Response 3 EE (%) |
|---|---|---|---|---|---|---|---|
| 6 | 1 | 12 | 14 | 2 | 184.48 | 0.2965 | 91.1 |
| 9 | 2 | 6.5 | 4 | 2 | 205.47 | 0.3125 | 93.91 |
| 2 | 3 | 12 | 4 | 3.5 | 176.84 | 0.3112 | 88.96 |
| 13 | 4 | 6.5 | 14 | 3.5 | 182.98 | 0.2311 | 75.47 |
| 1 | 5 | 1 | 4 | 3.5 | 200.92 | 0.259 | 80.1 |
| 8 | 6 | 12 | 14 | 5 | 152.81 | 0.1685 | 71.17 |
| 15 | 7 | 6.5 | 14 | 3.5 | 184.7 | 0.2411 | 75.46 |
| 7 | 8 | 1 | 14 | 5 | 182.63 | 0.1496 | 63.1 |
| 14 | 9 | 6.5 | 14 | 3.5 | 184.7 | 0.2411 | 78.1 |
| 4 | 10 | 12 | 24 | 3.5 | 164.7 | 0.2146 | 71.86 |
| 12 | 11 | 6.5 | 24 | 5 | 160.72 | 0.1312 | 59.11 |
| 10 | 12 | 6.5 | 24 | 2 | 185.21 | 0.2686 | 78.11 |
| 11 | 13 | 6.5 | 4 | 5 | 171.98 | 0.2101 | 75.25 |
| 5 | 14 | 1 | 14 | 2 | 208.23 | 0.3012 | 80.15 |
| 3 | 15 | 1 | 24 | 3.5 | 199.35 | 0.191 | 64.21 |

**Table 3. ANOVA for Particle Size**

| Source | Sum of Square | Df | Mean Square | *F*-value | p-value | Significance |
|---|---|---|---|---|---|---|
| **Model** | 3492.45 | 3 | 1164.15 | 83.96 | <0.0001 | Significant |
| A-oil | 1576.41 | 1 | 1576.41 | 113.69 | <0.0001 | |
| B- | 255.72 | 1 | 255.72 | 18.44 | 0.0013 | |
| C-sonication time | 1660.32 | 1 | 1660.32 | 119.75 | <0.0001 | |
| **Residual** | 152.52 | 11 | 13.87 | | | |
| Lack of fit | 150.55 | 9 | 16.73 | 16.96 | 0.0569 | Not significant |
| Pure error | 1.97 | 2 | 0.9861 | | | |
| Cor. total | 3644.97 | 14 | | | | |

**Table 4. ANOVA for PDI**

| Source | Sum of Square | Df | Mean Square | *F*-value | *p*-value | Significance |
|---|---|---|---|---|---|---|
| **Model** | 0.0451 | 3 | 0.0150 | 75.99 | <0.0001 | significant |
| A- Oil | 0.0010 | 1 | 0.0010 | 5.12 | 0.0448 | |
| B-$S_{mix}$ | 0.0103 | 1 | 0.0103 | 52.24 | <0.0001 | |
| C- Sonication time | 0.0337 | 1 | 0.0337 | 170.61 | <0.0001 | |
| **Residual** | 0.0022 | 11 | 0.0002 | | | |
| Lack of fit | 0.0021 | 9 | 0.0002 | 7.03 | 0.1308 | not significant |
| Pure error | 0.0001 | 2 | 0.0000 | | | |
| **Cor. total** | 0.0472 | 14 | | | | |

**Table 5. ANOVA for EE %**

| Source | Sum of Square | Df | Mean Square | *F*-value | *p*-Value | Significance |
|---|---|---|---|---|---|---|
| **Model** | 1381.18 | 3 | 460.39 | 610.24 | <0.0001 | Significant |
| A- Oil | 157.80 | 1 | 157.80 | 209.16 | <0.0001 | |
| B-$S_{mix}$ | 526.99 | 1 | 526.99 | 698.52 | <0.0001 | |
| C- Sonication time | 696.39 | 1 | 696.39 | 923.06 | <0.0001 | |
| **Residual** | 8.30 | 11 | 0.7544 | | | |
| Lack of fit | 3.67 | 9 | 0.4078 | 0.1762 | 0.9746 | Not significant |
| Pure error | 4.63 | 2 | 2.31 | | | |
| **Cor. total** | 1389.48 | 14 | | | | |

formulation. The reduction in the melting point may also indicate partial amorphization, which can enhance the bioavailability and dissolution rate of the active components. Furthermore, the altered thermal behavior reflects the effective integration of mannitol into the nanoemulsion matrix, which improves its compatibility and stability within the system. These merits demonstrate that the observed shift is advantageous rather than detrimental.

The absence of the characteristic endothermic peaks of both Piracetam (147.42 °C) and Shatavarin IV (216.59 °C) in the nanoemulsion thermogram suggests that these active ingredients are no longer in their crystalline forms within the formulation. This disappearance of the distinct melting points indicated that Piracetam and Shatavarin IV have been successfully incorporated into the nanoemulsion matrix, potentially in an amorphous or solubilized state. Furthermore,



https://doi.org/10.1021/acsomega.4c09072
ACS Omega 2025, 10, 9132−9153

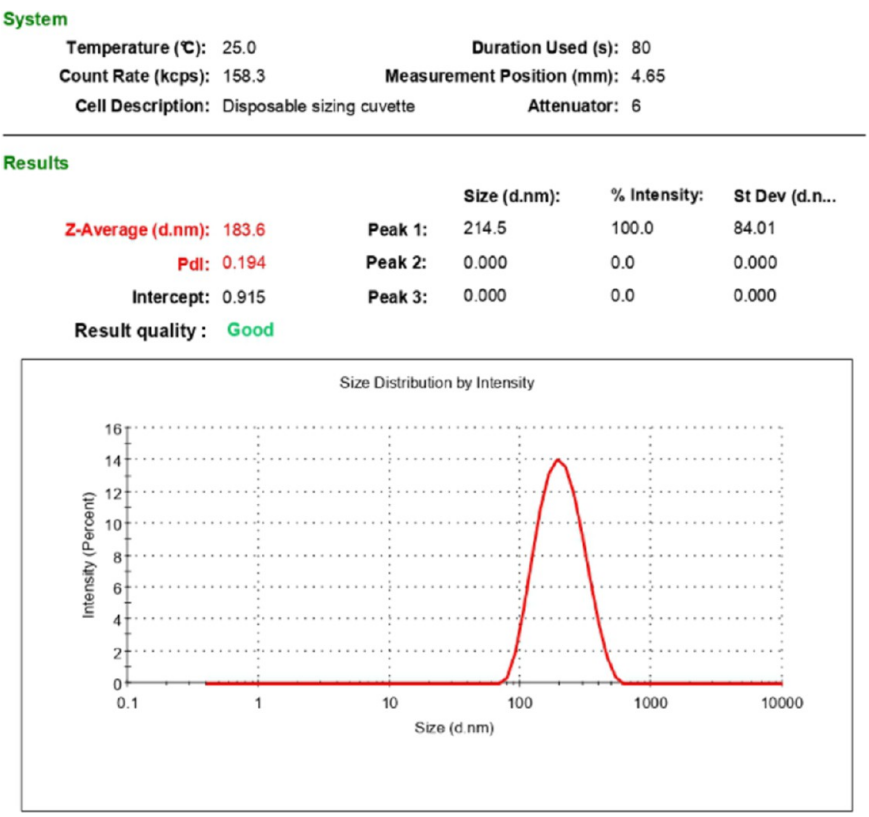


**Figure 11.** *Z*-Average, PDI, and size distribution by intensity graph.

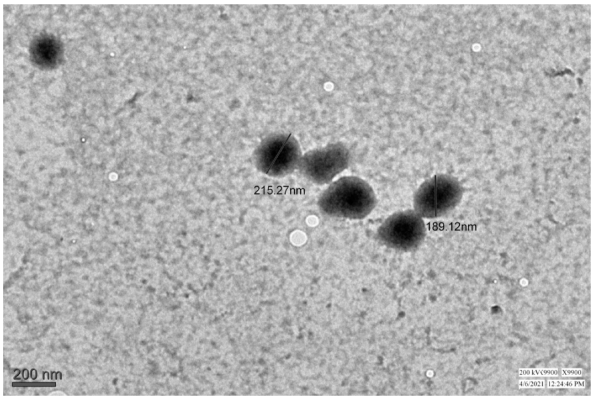


**Figure 12.** TEM of PSNE.

the lack of any new or additional peaks in the thermogram of the nanoemulsion formulation confirms that there are no significant interactions or incompatibilities between the drugs (Piracetam and Shatavarin IV) and the formulation excipients, including mannitol. PSNE maintained the stability of both active pharmaceutical ingredients without any undesirable interactions, thereby preserving the efficacy and integrity of the final product and likely enhancing the solubility and bioavailability, which are essential for their intended therapeutic use. These findings align with previous studies, which also reported the disappearance of crystalline peaks indicating amorphization of the drug and enhanced stability.[55,56] This is consistent with the observation that nanoemulsions can improve solubility and dissolution rates through the conversion of crystalline drugs into an amorphous state.[57]

*3.5.4. FTIR.* The FTIR spectra of Piracetam, Shatavarin IV, and the nanoemulsion formulation demonstrate key functional group similarities and differences. Piracetam's spectrum shows characteristic peaks for N−H stretching at 2996 $cm^{-1}$, C = O stretching at 1591 $cm^{-1}$, and C−N stretching around 1398 $cm^{-1}$, confirming its lactam structure. Shatavarin IV exhibits broad O−H stretching at 2993 $cm^{-1}$, strong C═O stretching between 1588 and 1680 $cm^{-1}$, and distinct C−O−C stretching from 1275 to 1009 $cm^{-1}$, reflecting its saponin structure with glycosidic linkages. In the nanoemulsion, the spectrum retains key features from both drugs with broad O−H/N−H stretching at 2997 $cm^{-1}$ and C═O stretching at 1672 $cm^{-1}$, indicating that both Piracetam and Shatavarin IV are incorporated into the formulation. The broad O−H peak suggests enhanced hydrogen bonding, crucial for nanoemulsion stability, while the absence of significant shifts or new peaks confirms the drugs' chemical integrity within the formulation. Overall, the FTIR analysis verifies that the nanoemulsion successfully encapsulates both active ingredients without compromising their functional groups, ensuring stability and efficacy of the formulation (Figure 14). This analysis supports the compatibility of the individual formulation components as a drug delivery system, as previous studies indicated.[58,59]

**3.6. *In Vitro* Drug Release.** The *in vitro* drug release profile of PSNE and the drug suspension, as depicted in Figure 15, showed a significant difference in the % CDR over time between the two formulations. PSNE demonstrates a much faster and more sustained release, reaching 84.30 ± 1.03% CDR within 24 h, whereas the drug suspension achieves only about 31.79 ± 0.89% release over the same period. The initial phase of the release from the nanoemulsion is rapid, with a steep increase in % CDR within the first few hours, indicating


https://doi.org/10.1021/acsomega.4c09072
ACS Omega 2025, 10, 9132−9153

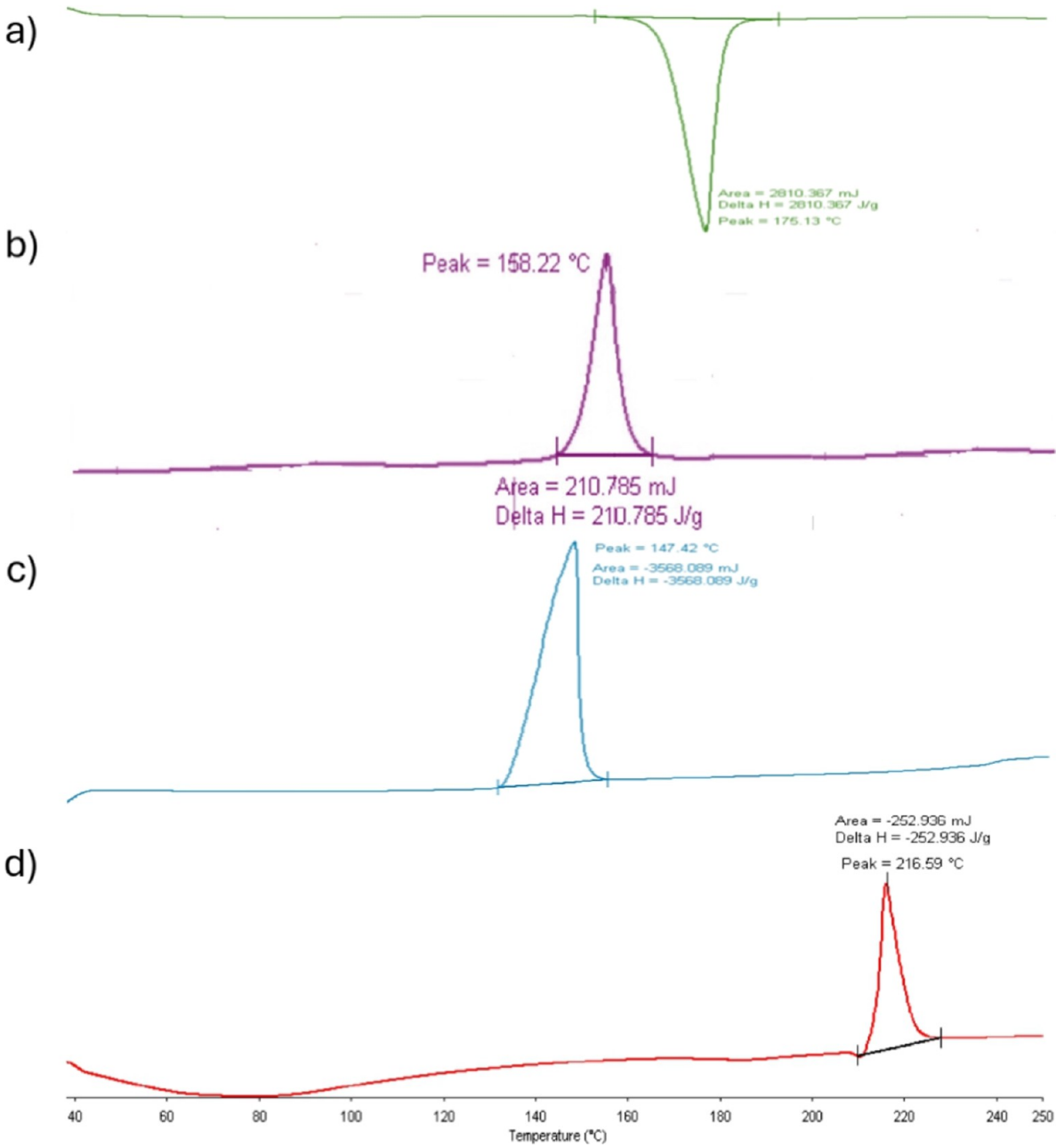


**Figure 13.** DSC of (a) Piracetam, (b) mannitol, (c) PSNE, and (d) Shatavarin.

an initial burst release of the drug from the nanoemulsion droplets. PSNE followed the Higuchi model, as evidenced by the $R^2$ value of 0.9512. The high $R^2$ value (close to 1) indicated a strong correlation and a good fit of the release data to the Higuchi kinetic model. This suggested that the drug release from the nanoemulsion is primarily governed by a diffusion-controlled mechanism, where the drug molecules diffuse out of the formulation matrix into the surrounding medium. Overall, PSNE significantly enhances the release rate compared to the conventional suspension, likely due to its smaller droplet size, higher surface area, and improved solubility. The calibration curve of absorbance versus concentration with the regression equation was y = 0.0154x + 0.0122, and a correlation coefficient was observed to be $R^2$ = 0.9971, and the UV spectrum of the analyte showed a $\lambda_{max}$ at 214 nm.

**3.7. *Ex Vivo* Drug Permeation.** The *ex vivo* drug permeability graph compared the permeability profiles of PSNE and a conventional drug suspension through gut tissue over 4 h (Figure 16). PSNE demonstrated a rapid increase in permeability, reaching 56.35 ± 1.19% within the first 4 h, whereas the drug suspension achieves only 30.39 ± 0.66% permeability over the same duration. The initial phase shows a sharp rise in the percentage permeability for the nanoemulsion, with most of the permeability occurring within the first hour, suggesting a quick initial absorption phase. In contrast, the drug suspension exhibited a slower and more gradual increase in permeability, reflecting a limited penetration across the gut tissue. This difference in permeability between the two formulations can be attributed to the PSNE's smaller droplet size, which increased the surface area for absorption, and its ability to enhance drug solubility and stability in the gut


https://doi.org/10.1021/acsomega.4c09072
ACS Omega 2025, 10, 9132−9153

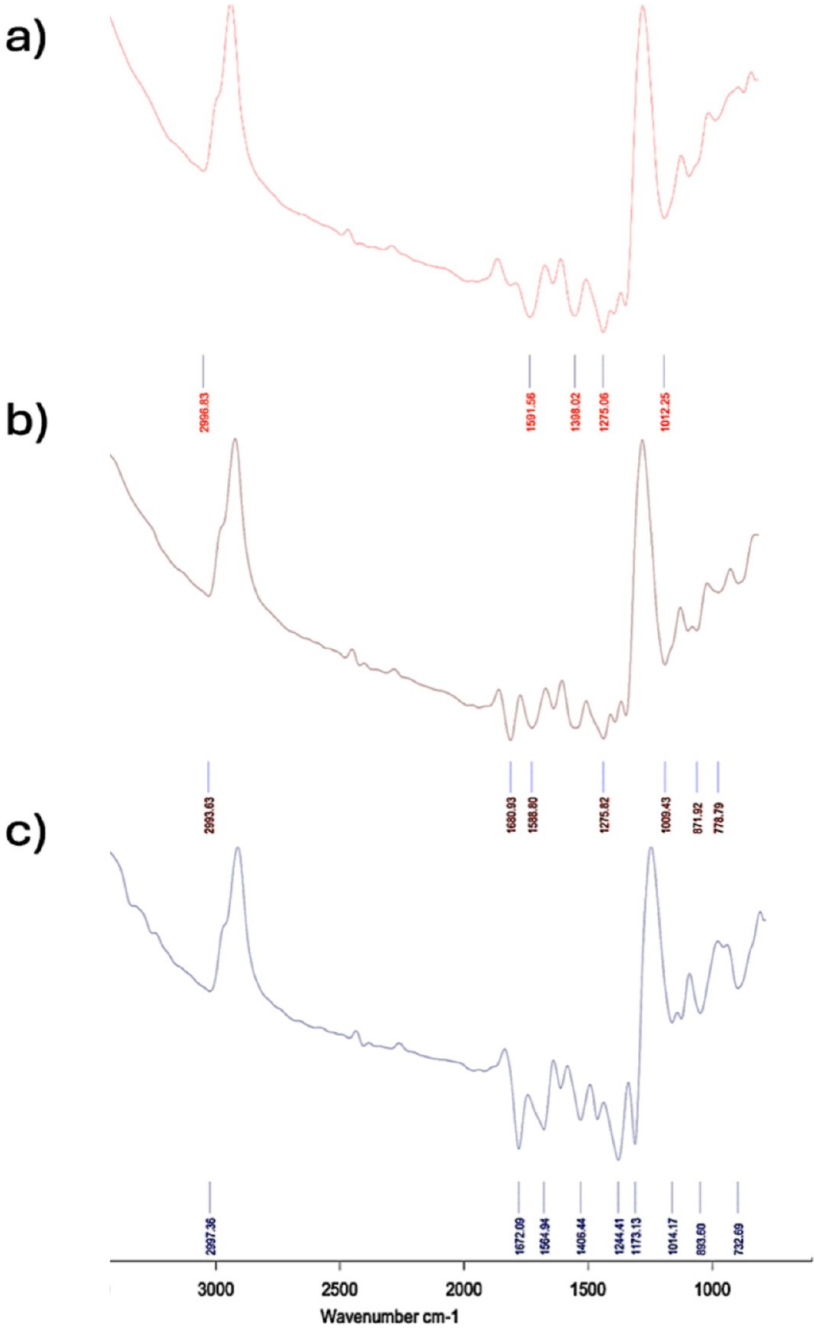


**Figure 14.** FTIR spectra of (a) Piracetam, (b) Shatavarin, and (c) PSNE.

environment. The higher permeability observed with the PSNE indicated that it facilitated more efficient transport of Piracetam and Shatavarin IV across the gut membrane, likely due to its ability to enhance drug solubility, reduce interfacial tension, and improve the interaction with the biological membrane. The graph illustrates the cumulative amount of CADP permeated over time for both the formulation and the suspension. The CADP formulation demonstrates a significantly higher permeation rate compared to the suspension, indicating its superior drug delivery efficacy. By 4 h, the permeation for the formulation is nearly double that of the suspension, emphasizing its enhanced permeability. The permeability coefficient (Kp) for this study was found to be 3.789 ($cm^{-2}$ $h^{-1}$), supporting the efficiency of the CADP formulation in drug permeation (Figure 17).

**3.8. MTT Cell Line Assay.** Piracetam, Shatavarin IV, and PSNE exhibited a wide range of inhibition against N2A cell lines in a dose-dependent manner. For Piracetam, Figure 18a shows a gradual decrease in cell viability with increasing concentrations. At lower concentrations (0.97−62.50 $\mu$g/mL), Piracetam exhibits minimal cytotoxicity, with cell viability remaining above 70%. However, as the concentration increases beyond 125 $\mu$g/mL, a steady decline in cell viability is observed, reaching approximately 20−30% at the highest concentration of 2000 $\mu$g/mL. The corresponding line graph (Figure 18b) further confirms this trend, showing a steep decline in % cell viability beyond 1000 $\mu$g/mL. This indicated that Piracetam exerted dose-dependent cytotoxicity, particularly at higher concentrations.



https://doi.org/10.1021/acsomega.4c09072
ACS Omega 2025, 10, 9132−9153

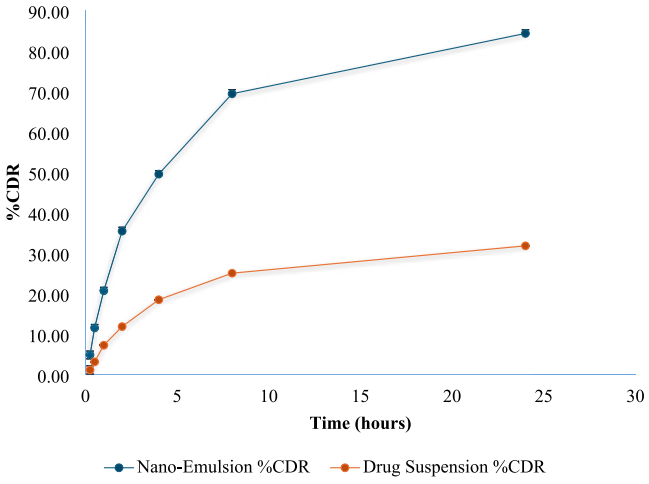


**Figure 15.** *In vitro* analysis of PSNE.

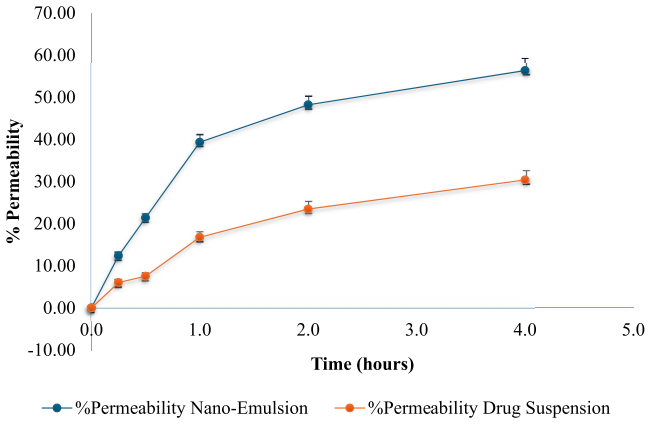


**Figure 16.** Ex vivo drug permeation of PSNE.

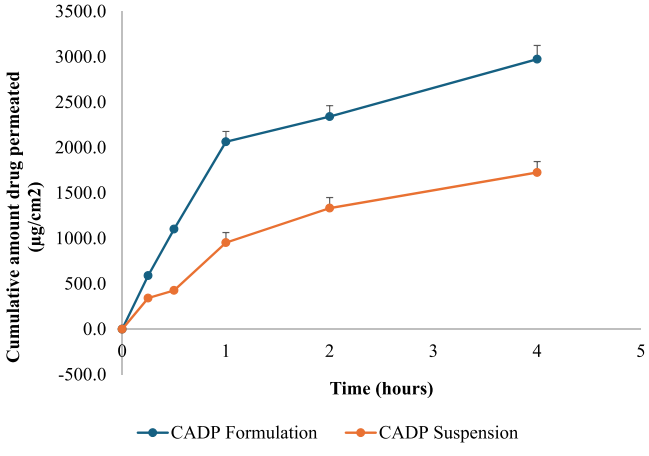


**Figure 17.** Cumulative amount drug permeated comparison between formulation and suspension.

Similarly, Shatavarin IV displayed a dose-dependent decrease in cell viability. Figure 18c highlights that at lower concentrations (0.97−31.25 μg/mL), cell viability remained relatively high, approximately 70−80%. However, a sharp decline begins at concentrations above 62.5 μg/mL, with cell viability dropping to 20−30% at the highest concentrations (1000−2000 μg/mL). This pattern was reinforced by Figure 18d, where a rapid decrease in cell viability was observed beyond the 500 μg/mL mark. These observations suggested that Shatavarin IV, like Piracetam, demonstrated significant cytotoxicity in a concentration-dependent manner.

The nanoemulsion formulation (PSNE) combining Piracetam and Shatavarin IV showed an enhanced cytotoxic effect compared with the individual compounds. In Figure 18e, cell viability remained high (∼70−80%) at lower concentrations (0.97−31.25 μg/mL). However, as the concentrations increased beyond 62.5 μg/mL, a significant drop in cell viability is observed. At higher concentrations (1000−2000 μg/mL), PSNE reduced cell viability to 20−30%, demonstrating greater cytotoxicity than either Piracetam or Shatavarin IV alone. Figure 18f further illustrates this trend, showing a faster and more pronounced decline in % cell viability as the concentration increases. This suggested that the nanoemulsion formulation enhances cytotoxic potential, likely due to improved solubility, cellular uptake, and bioavailability of the drugs. Based on the MTT assay results, the $IC_{50}$ values (μg/mL) for Piracetam and Shatavarin IV after 24 h of treatment at 37 °C with 5% $CO_2$ were found to be 125 μg/mL and 62.5 μg/mL, respectively. The results were statistically significant ($p < 0.05$*), supporting the dose-dependent inhibition observed. Previous studies report that Piracetam at 1 mM concentration demonstrated cytoprotective effects in astrocyte cultures subjected to hypoxia. The MTT assay, among other methods, showed that Piracetam reduced cell death, decreased apoptotic markers, and enhanced mitochondrial function during hypoxia and reoxygenation periods.[60] On the other hand, Piracetam did not exhibit cytotoxic effects up to a concentration of 10 mM in hypoxic V79 cells. It also had no significant impact on the radiosensitivity of these cells, as evaluated by both MTT and clonogenic assays.[61] Simultaneously, prior research observed that the MTT assay showed that a Shatavarin-rich fraction had potent cytotoxic effects, with additional *in vivo* evidence suggesting tumor-reducing properties in mouse models in dose-dependent manner, indicating enhanced cell viability in the presence of the compound during oxidative stress conditions.[62,63] Studies comparing MTT assay results with other cytotoxicity assays, such as SRB- and ATP-based assays, suggest that MTT provides reliable results for Shatavarin IV but may sometimes underestimate cytotoxic effects compared to ATP assays, depending on experimental conditions.[64]

**3.9. Antioxidant Assay.** PSNE exhibited a stronger antioxidant effect than that of the pure extract. However, the difference in the antioxidant activity between PSNE and ascorbic acid was not statistically significant. There was, however, a significant difference between the antioxidant activity of PSNE and the pure extract. The DPPH assay, based on the reduction of absorbance at 517 nm due to the scavenging of DPPH radicals by antioxidants, showed that the $IC_{50}$ value for PSNE was 135.07 ± 0.36, while the $IC_{50}$ values for ascorbic acid and Shatavari extract were 45 ± 0.53 and 119.45 ± 0.25, respectively (Table 6). Previous research has highlighted the antioxidant properties of both Piracetam and Shatavarin, demonstrating significant activity individually, which further reinforces their synergistic antioxidant potential.[65,66]

**3.10. pH and Stability Analysis of PSNE.** Table 7 demonstrates the behavior of the nanoemulsion formulation over time at different temperatures (5 °C, 25 °C, and 40 °C) in terms of droplet size, PDI, zeta potential, pH, and conductivity. Over time, the droplet size slightly increased at all temperatures, with the largest sizes recorded at 40 °C, while the PDI



https://doi.org/10.1021/acsomega.4c09072
ACS Omega 2025, 10, 9132−9153

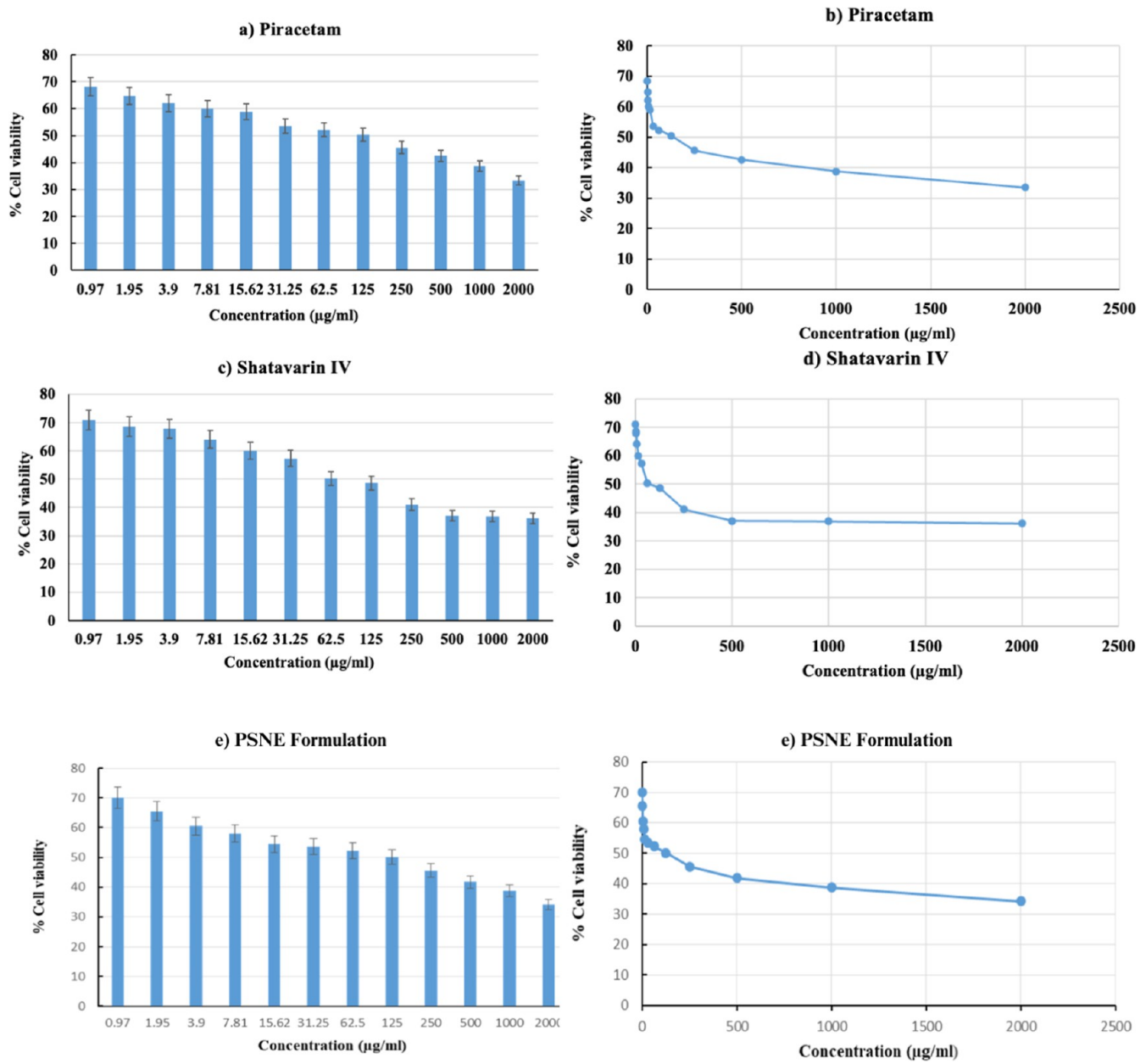


**Figure 18.** MTT cell line assay.

**Table 6. $IC_{50}$ of Formulations**

| S.No. | Sample | $IC_{50}$ µg/mL |
|---|---|---|
| 1 | Shatavari extract | 119.45 ± 0.25 |
| 2 | Shatavari nanoemulsion | 135.07 ± 0.36 |
| 3 | Standard ascorbic acid | 45 ± 0.53 |

also showed a gradual increase, indicating a broader PDI, especially at higher temperatures. The zeta potential became more negative, which could suggest improved colloidal stability. Minimal pH fluctuations were observed, with a slight decrease at 5 and 25 °C. Conductivity increased across all conditions, particularly at higher temperatures, indicating potential changes in the ionic environment of the nanoemulsion. Overall, the formulation remained stable, although the higher temperatures induced more pronounced changes in particle characteristics.

The synergistic effects observed in this study align with previous reports where combination therapies demonstrated enhanced efficacy in addressing the multifactorial nature of AD. For instance, nanoemulsions have been shown to improve drug bioavailability and BBB penetration in similar contexts.[67] The superior permeability and antioxidant activity observed in this study further substantiate the potential of nanoemulsions as a delivery vehicle for AD therapies.[68] Future studies should include *in vivo* investigations and clinical validation to confirm these findings and explore long-term safety and efficacy.

## 4. CONCLUSIONS

The innovative aspects of this study included the novel combination of PSNE, which leverages their complementary mechanisms for a synergistic approach to Alzheimer's therapy. Furthermore, the use of nanoemulsion technology for brain-targeted delivery and enhanced bioavailability addresses critical


https://doi.org/10.1021/acsomega.4c09072
ACS Omega 2025, 10, 9132−9153

Table 7. pH, Rheological Parameters, and Stability Analysis of PSNE

| Temperature (°C) | Time (days) | Droplet Size (nm) | PDI | Zeta Potential (mV) | pH | Conductivity (μs/cm) |
|---|---|---|---|---|---|---|
| 5 | 30 | 170 ± 2.45 | 0.1400 ± 0.02 | −19.12 ± 0.83 | 4.70 ± 0.03 | 80.25 ± 1.50 |
| 5 | 60 | 185 ± 1.35 | 0.1450 ± 0.05 | −20.10 ± 0.75 | 5.00 ± 0.02 | 84.50 ± 2.55 |
| 5 | 90 | 183 ± 2.45 | 0.1600 ± 0.06 | −21.00 ± 0.93 | 4.90 ± 0.07 | 88.00 ± 1.75 |
| 5 | 180 | 182 ± 1.80 | 0.1800 ± 0.02 | −21.50 ± 0.55 | 4.55 ± 0.02 | 87.30 ± 1.89 |
| 25 | 30 | 178 ± 2.23 | 0.1750 ± 0.12 | −19.50 ± 1.64 | 5.05 ± 0.02 | 93.25 ± 1.20 |
| 25 | 60 | 189 ± 2.40 | 0.1400 ± 0.07 | −20.05 ± 1.03 | 4.50 ± 0.01 | 100.10 ± 2.00 |
| 25 | 90 | 186 ± 2.05 | 0.1505 ± 0.06 | −20.25 ± 1.35 | 4.85 ± 0.04 | 125.05 ± 1.65 |
| 25 | 180 | 186 ± 0.60 | 0.1410 ± 0.19 | −20.00 ± 1.10 | 4.12 ± 0.09 | 124.75 ± 1.25 |
| 40 | 30 | 188 ± 0.95 | 0.1550 ± 0.02 | −21.10 ± 0.83 | 4.75 ± 0.01 | 105.50 ± 1.60 |
| 40 | 60 | 182 ± 2.90 | 0.1820 ± 0.07 | −19.50 ± 1.45 | 4.82 ± 0.04 | 108.25 ± 2.50 |
| 40 | 90 | 191 ± 0.60 | 0.1650 ± 0.04 | −20.15 ± 0.77 | 5.02 ± 0.02 | 92.85 ± 2.10 |
| 40 | 180 | 190 ± 0.85 | 0.1700 ± 0.35 | −19.85 ± 0.50 | 5.15 ± 0.25 | 90.25 ± 2.15 |

limitations in current AD treatment strategies. The PSNE offered a promising synergistic formulation with improved drug delivery properties and potent antioxidant activity. It improved the solubility of both Piracetam and Shatavarin IV, which are typically poorly water-soluble compounds. The smaller droplet size and increased surface area of the nanoemulsion contribute to better drug dissolution and absorption, enhancing the bioavailability. The combination of Piracetam and Shatavarin IV in PSNE exhibited a synergistic effect, indicating enhanced therapeutic efficacy. Additional research is required to evaluate the pharmacokinetics, pharmacodynamics, and long-term safety profile of the PSNE. PSNE formulations could be investigated for use in other neurological disorders, where similar therapeutic mechanisms may be beneficial.

## ■ ASSOCIATED CONTENT

### Data Availability Statement

The data generated during this study has been added throughout the manuscript.

## ■ AUTHOR INFORMATION


### Corresponding Author

**Abul Kalam Najmi** − *Department of Pharmacology. School of Pharmaceutical Education and Research, Jamia Hamdard, New Delhi 110062, India;* orcid.org/0000-0002-9299-414X; Phone: +91 9891220056; Email: aknajmi@jamiahamdard.ac.in

### Authors

**Mohd Nadeem** − *Department of Pharmacology. School of Pharmaceutical Education and Research, Jamia Hamdard, New Delhi 110062, India;* orcid.org/0009-0009-4521-9894

**Haya Majid** − *Department of Translational and Clinical Research, School of Chemical and Life Sciences, Jamia Hamdard, New Delhi 110062, India;* orcid.org/0000-0003-1439-1172

**Mohd Danish Ansari** − *Department of Pharmaceutical Technology, Faculty of Pharmacy, Universiti Malaya, Kuala Lumpur 50603, Malaysia;* orcid.org/0009-0006-4035-5377

**Farhan Jalees Ahmad** − *Department of Pharmaceutics, School of Pharmaceutical Education and Research, Jamia Hamdard, New Delhi 110062, India;* orcid.org/0000-0002-0740-8573

**Suhel Parvez** − *Department of Medical Elementology and Toxicology, School of Chemical and Life Sciences, Jamia Hamdard, New Delhi 110062, India;* orcid.org/0000-0002-6318-6506

**Mohd Akhtar** − *Department of Pharmacology. School of Pharmaceutical Education and Research, Jamia Hamdard, New Delhi 110062, India*

**Sayeed Ahmad** − *Department of Pharmacognosy and Phytochemistry, School of Pharmaceutical Education and Research, Jamia Hamdard, New Delhi 110062, India;* orcid.org/0000-0003-1573-152X

Complete contact information is available at: https://pubs.acs.org/10.1021/acsomega.4c09072


### Author Contributions

M.N. and A.K.N. contributed to experimental design and data collection. F.J.A., S.P., S.A., and M.A. assisted in data analysis and interpretation. H.M. and M.D.A wrote the main manuscript text. A.K.N., M.D.A., and H.M. provided critical revisions and intellectual input. A.K.N. coordinated the study, supervised the research, and contributed to manuscript preparation.


### Funding

The study was funded by the Indian Council of Medical Research, New Delhi, under the reference no. 45/61/2020-NANO/BMS.


### Notes

The authors declare no competing financial interest.

Ethics approval: the animals utilized in this study were sourced from the Central Animal House at Jamia Hamdard, situated in Delhi, India. The research adhered to ethical guidelines and received approval from the Institutional Animal Ethics Committee (IAEC) under registration no. CAHF: 1772, issued on December 21, 2020. The study was conducted in strict accordance with the guidelines established by the Committee for Control and Supervision of Experiments on Animals (CCSEA), registered as 173/GO/ReBi/S/2000/CPCSEA.


## ■ ACKNOWLEDGMENTS

The authors would like to express their gratitude to the Indian Council of Medical Research (ICMR) for their invaluable support in facilitating this research.




https://doi.org/10.1021/acsomega.4c09072
ACS Omega 2025, 10, 9132−9153

## REFERENCES


(1) Alzheimer's Disease Statistics & Facts (2023 Update). https://cfah.org/alzheimers-dementia-statistics/. (accessed Apr 28 2024).
(2) International A. D.. *World Alzheimer Report 2023: Reducing Dementia Risk: Never too early, never too late*, 2023.
(3) Kiraly, M.; Foss, J. F.; Giordano, T. Neuroinflammation, Its Role in Alzheimer's Disease and Therapeutic Strategies. *J Prev Alzheimers Dis.* **2023**, *10* (4), 686−698.
(4) Helmes, E.; Bowler, J. V.; Merskey, H.; Munoz, D. G.; Hachinski, V. C. I. Rates of Cognitive Decline in Alzheimer's Disease and Dementia with Lewy Bodies. *Dementia Geriatr. Cognit. Disord.* **2003**, *15*, 67−71.
(5) Ibrahim, M. M.; Gabr, M. T. Multitarget therapeutic strategies for Alzheimer's disease. *Neural Regener. Res.* **2019**, *14*, 437−440.
(6) Khan, W. U.; Salman, M.; Ali, M.; Majid, H.; Yar, M. S.; Akhtar, M.; Parvez, S.; Najmi, A. K. Neuroprotective Effects of Sulforaphane in a Rat Model of Alzheimer's Disease Induced by A$\beta$ (1−42) Peptides. *Neurochem. Int.* **2024**, *179*, 105839.
(7) Nodirahon, A.; Majid, H.; Waghdhare, S.; Vohora, D. The effect of sodium glucose Co-transport 2 inhibitors on cognitive impairment and depression in type 2 diabetes mellitus patients. *Clin. Epidemiol. Global Health* **2024**, *26*, 101555.
(8) Johnson, D. K.; Storandt, M.; Morris, J. C.; Galvin, J. E. Longitudinal study of the transition from healthy aging to Alzheimer disease. *Arch. Neurol.* **2009**, *66*, 1254−1259.
(9) Majid, H.; Verma, N.; Bhandari, S.; Gupta, S.; Nidhi. A Systematic Review on Safety and Efficacy of Migalastat for the treatment of Fabry's Disease. *Expert Opin. Pharmacother.* **2024**, *25*, 769−782.
(10) Perry, E.; Howes, M. J. R. Medicinal Plants and Dementia Therapy: Herbal Hopes for Brain Aging? *CNS Neurosci. Ther.* **2011**, *17*, 683−698.
(11) Hyde, A. J.; May, B. H.; Dong, L.; Feng, M.; Liu, S.; Guo, X.; Zhang, A. L.; Lu, C.; Xue, C. C. Herbal medicine for management of the behavioural and psychological symptoms of dementia (BPSD): A systematic review and meta-analysis. *J. Psychopharmacol.* **2017**, *31*, 169−183.
(12) Imran, M.; Riaz, T.; Majid, H.; Maqsood, S. Identification of botanicals using molecular biotechnology. *Polym. Med.* **2023**, *53*, 69−79.
(13) Majid, H.; Masoom, M.; Khan, M. A.; Garg, A. Safety and Efficacy of Genistein in Sanfilippo Syndrome-A Systematic Review. *Curr. Drug Ther.* **2023**, *18*, 323.
(14) Kwon, C. Y.; Lee, B. Herbal Medicine for Behavioral and Psychological Symptoms of Dementia: A Systematic Review and Meta-Analysis. *Front. Pharmacol* **2021**, *12*.713287.
(15) NeuroQuantology, M. A. undefined Asparagus Racemosus (Shatavari): A potent herbal plant for combating neurodegenerative diseases, 2022. search.proquest.com.
(16) Kashyap, P.; Muthusamy, K.; Niranjan, M.; Steroids, S. T. *undefined Sarsasapogenin: A steroidal saponin from Asparagus racemosus as multi target directed ligand in Alzheimer's disease*; Elsevier, 2020.
(17) Bhatnagar, M., Meena, P., Barbar, S. Undefined Neuroprotective response of the hippocampus region of the brain to Withania somnifera and Asparagus racemosus root extract: An in vitro study. academicjournals.org., 2013 (Accessed September 21, 2024).
(18) Khan, M. A.; Tyagi, K.; Masoom, M.; Majid, H.; Garg, A.; Bhurani, D.; Agarwal, N. B. Role of Cytokines in Chemotherapy-related Cognitive Impairment of Breast Cancer Patients: A Systematic Review. *Curr. Rev. Clin. Exp. Pharmacol.* **2023**, *18*, 110−119.
(19) Sharma, K.; Bhatnagar, M.; Kulkarni, S. *Effect of Convolvulus pluricaulis Choisy. and Asparagus racemosus Willd on learning and memory in young and old mice: A comparative evaluation*, 2010.
(20) Saxena, G., Singh, M. undefined Neuroprotective effects of Asparagus racemosus Linn root extract: an experimental and clinical evidence. annalsofneurosciences.org, 2010 (Accessed September 21, 2024).
(21) Majumdar, S.; Gupta, S. *undefined Neuro-nutraceutical potential of Asparagus racemosus: A review*; Elsevier, 2021.
(22) Hasan, N.; Ahmad, N.; Abdul, A. P. J.; Zohrameena, S.; Khalid, M. Asparagus racemosus: for medicinal uses & pharmacological actions. *Int. J. of Adv. Res.* **2016**, *4*, 259−267.
(23) Patel, J., King, A. undefined Understanding nootropics and cognitive enhancement: mechanism of action and ethical considerations. healthopenresearch.org., 2024 (Accessed September 21, 2024).
(24) Cohen, P. A.; Avula, B.; Wang, Y. H.; Zakharevich, I.; Khan, I. Five Unapproved Drugs Found in Cognitive Enhancement Supplements. *Nat. Clin. Pract.* **2021**, *11*, E303−E307.
(25) Leuner, K.; Kurz, C.; Guidetti, G.; Orgogozo, J. M.; Müller, W. E. Improved mitochondrial function in brain aging and Alzheimer disease - the new mechanism of action of the old metabolic enhancer piracetam. *Front. Neurosci.* **2010**, *1*.44.
(26) Croisile, B.; Trillet, M.; Fondarai, J.; Laurent, B.; Mauguière, F.; Billardon, M. Long-term and high-dose piracetam treatment of Alzheimer's disease. *Neurology* **1993**, *43*, 301−305.
(27) Flicker, L.; Grimley Evans, J. Piracetam for dementia or cognitive impairment. *Cochrane Database Syst. Rev.* **2004**, CD001011.
(28) Raghavendra, M.; Ali, P.; Rao Tadikonda, R.; Srikanth, S.; Rajesham, V. V.; Roshan Ali, P.; Rao, T. R.; Raghavendra, M. Evaluation of synergistic potential of insulin with piracetam against amyloid beta (1−42) induced cognitive impairment. *YMER* **2010**, *21* (11), 1947−1956.
(29) Eckert, G. P.; Cairns, N. J.; Müller, W. E. Piracetam reverses hippocampal membrane alterations in Alzheimer's disease. *J. Neural Transm.* **1999**, *106*, 757−761.
(30) Dahalia, M.; Gupta, S.; Majid, H.; Vohora, D.; Nidhi. Pirfenidone regulates seizures through the HMGB1/TLR4 axis to improve cognitive functions and modulate oxidative stress and neurotransmitters in PTZ-induced kindling in mice. *Front. Pharmacol* **2025**, *15*, 1528032.
(31) Bhatt, P. *A detailed review on nanoemulsion drug delivery system*. SM-IJ of P sciences, 2011 undefined; Citeseer 2, 2011.
(32) Azeem, A.; Rizwan, M.; Ahmad, F.; Iqbal, Z.; Pharmscitech, R. K.-A. *Nanoemulsion components screening and selection: a technical note*; Springer, 2009.
(33) Jaiswal, M.; Dudhe, R. *Nanoemulsion: an advanced mode of drug delivery system*. Biotech PS-3, 2015 undefined; Springer, 2015; Vol. *5*, pp 123−127.
(34) Kulkarni, G. T.; Sharma, N.; Bansal, M.; Visht, S.; Sharma, P. K.; Kulkarni, G. T. Nanoemulsion: A new concept of delivery system. *Chronicles of Young Scientists* **2010**, *1* (2), 2−6.
(35) Singh, Y.; Meher, J.; Raval, K. *FK-J of controlled, undefined Nanoemulsion: Concepts, development and applications in drug delivery*; Elsevier, 2017.
(36) Azeem, A.; Rizwan, M.; Ahmad, F. J.; Iqbal, Z.; Khar, R. K.; Aqil, M.; Talegaonkar, S. Nanoemulsion components screening and selection: A technical note. *AAPS PharmSciTech* **2009**, *10*, 69−76.
(37) Patel, R. *An overview on nanoemulsion: a novel approach*. JJ-IJ of PS, 2012 undefined; Citeseer 3, 2012.
(38) Shah, P.; Bhalodia, D. *PS-S reviews, 2010 undefined Nanoemulsion: A pharmaceutical review*; Systematic Reviews in Pharmacy, 2010. ebscohost.com.
(39) Pasha, S.; Khanam, S.; Afsar, Z. ISOLATION AND CHARACTERIZATION OF CHEMICAL CONSTITUENTS OF ASPARAGUS RACEMOSUS AS MARKERS. *Int. J. Res. Dev. Pharm. Life Sci.*, *5*, 2255−2263.
(40) Imran, M.; Majid, H.; Ali, M.; Qadir, A. Phytochemical screening of Solanum xanthocarpum and its xanthine oxidase inhibitory activity. *Prog. Nucl. Energy 6 Biol. Sci.* **2022**, *02*.311.
(41) Patil, P. R.; Bhurat, M. R.; Sanghavi, R. S.; Nagdev, S. A.; Patil, P. R. HPTLC FINGERPRINTING AND QUANTIFICATION OF SHATAVARIN IV IN EXTRACT AND POLYHERBAL FORMULATIONS. *World J. Pharmaceut. Res.* **2018**, *7*, 442.
(42) Alam, P.; Alam, A.; Anwer, M. K.; Alqasoumi, S. I. Quantitative estimation of hesperidin by HPTLC in different varieties of citrus peels. *Asian Pac. J. Trop. Biomed.* **2014**, *4*, 262−266.




https://doi.org/10.1021/acsomega.4c09072
*ACS Omega* 2025, 10, 9132−9153

(43) Shakeel, F.; Alam, P.; Anwer, M. K.; Alanazi, S. A.; Alsarra, I. A.; Alqarni, M. H. Wound healing evaluation of self-nanoemulsifying drug delivery system containing Piper cubeba essential oil. *3 Biotech* **2019**, *9*, 82.
(44) Hasan, N.; Imran, M.; Nadeem, M.; Jain, D.; Haider, K.; Moshahid Alam Rizvi, M.; Sheikh, A.; Kesharwani, P.; Kumar jain, G.; Jalees Ahmad, F. Formulation and development of novel lipid-based combinatorial advanced nanoformulation for effective treatment of non-melanoma skin cancer. *Int. J. Pharm.* **2023**, *632*, 122580.
(45) Alamdari, S.; Ghamsari, M. S.; Tafreshi, M. Synthesis, characterization, and gas sensing properties of In-doped ZnO nanopowders. *Nanochem Res.* **2017**, *2*, 198.
(46) Ding, B.; Zhang, X.; Hayat, K.; Xia, S.; Jia, C.; Xie, M.; Liu, C. Preparation, characterization and the stability of ferrous glycinate nanoliposomes. *J. Food Eng.* **2011**, *102*, 202−208.
(47) Alam, P.; Imran, M. A.; Ali, A.; Majid, H. Cananga odorata (Ylang-Ylang) Essential Oil Containing Nanoemulgel for the Topical Treatment of Scalp Psoriasis and Dandruff. *Gels* **2024**, *10*, 303.
(48) Alam, P.; Imran, M. A.; Ahmed, S.; Majid, H.; Akhtar, A. Chitosan Nanoparticles for Enhanced Delivery of Sida cordifolia Extract: Formulation, Optimization and Bioactivity Assessment. *Pharmaceuticals* **2023**, *16*, 1561.
(49) Mutalik, S. P.; Mullick, P.; Pandey, A.; Kulkarni, S. S.; Mutalik, S. Box−Behnken design aided optimization and validation of developed reverse phase HPLC analytical method for simultaneous quantification of dolutegravir sodium and lamivudine co-loaded in nano-liposomes. *J. Sep. Sci.* **2021**, *44*, 2917−2931.
(50) Li, J.; Guo, R.; Hu, H.; Wu, X.; Ai, L.; Wu, Y. Preparation optimization and storage stability of nanoemulsion-based lutein delivery systems. *J. Microencapsul.* **2018**, *35*, 570−583.
(51) Zintle, M.; Siwaphiwe, P.; Marthe Carine, F.; Thierry Youmbi, F.; Derek Tantoh, N.; Suprakas Sinha, R.; Blessing Atim, A. Antibacterial study of Carbopol-mastic gum/silver nanoparticle-based topical gels with carvacrol/neem bark extract in vitro. *J. Wound Care* **2023**, *32* (Sup9a), Sup9a.
(52) Kamran, M.; Ahad, A.; Aqil, M.; Imam, S. S.; Sultana, Y.; Ali, A. Design, formulation and optimization of novel soft nano-carriers for transdermal olmesartan medoxomil delivery: In vitro characterization and in vivo pharmacokinetic assessment. *Int. J. Pharm.* **2016**, *505*, 147−158.
(53) Altuntas, E.; Yener, G. Anti-aging potential of a cream containing herbal oils and honey: Formulation and in vivo evaluation of effectiveness using non-invasive biophysical techniques. *J. Pharm. Biol. Sci.* **2015**, *10*, 51−60.
(54) Qadir, A.; Faiyazuddin, M. D.; Talib Hussain, M. D.; Alshammari, T. M.; Shakeel, F. Critical steps and energetics involved in a successful development of a stable nanoemulsion. *J. Mol. Liq.* **2016**, *214*, 7−18.
(55) Rungsanga, T., Tuntijarukornb, P., Asia, K. I.-S.. Stability and clinical effectiveness of emulsion containing Asparagus racemosus root extract, 2015. thaiscience.info (Accessed September 21, 2024).
(56) Picciochi, R.; Diogo, H. P.; Minas Da Piedade, M. E. Thermodynamic Characterization of Three Polymorphic Forms of Piracetam. *J. Pharm. Sci.* **2011**, *100*, 594−603.
(57) Manyarara, T. E.; Khoza, S.; Dube, A.; Maponga, C. C. Formulation and characterization of a paediatric nanoemulsion dosage form with modified oral drug delivery system for improved dissolution rate of nevirapine. *MRS Adv.* **2018**, *3*, 2203−2219.
(58) Karamancheva, I.; Staneva, T. Determination of possible impurities in piracetam using FTIR spectroscopy. *J. Pharm. Biomed. Anal.* **2000**, *21*, 1161−1169.
(59) Pandey, V.; Shri, M.; Dubey, S.; Saema, S.; Tiwari, S. An Insight of Phytochemicals of Shatavari (Asparagus racemosus). *Plants for Immunity and Conservation Strategies* **2023**, 169−205.
(60) Gabryel, B.; Adamek, M.; Pudełko, A.; Małecki, A.; Trzeciak, H. I. Piracetam and vinpocetine exert cytoprotective activity and prevent apoptosis of astrocytes in vitro in hypoxia and reoxygenation. *Neurotoxicology* **2002**, *23* (1), 19−31.
(61) Lagarde, P.; Gheuens, E. E. O.; De Pooter, C. M. J.; De Bruijn, E. A.; van der Heyden, S.; Chomy, F.; Van Oosterom, A. T.; Scalliet, P. G. Effets in vitro du piracetam sur la radiosensibilité des cellules hypoxiques (adaptation du test au MTT aux conditions d'hypoxie). *Bull. Cancer* **1995**, *82*, 929−938.
(62) Jadaun, P.; Harshithkumar, R.; Seniya, C.; Gaikwad, S. Y.; Bhoite, S. P.; Chandane-Tak, M.; Borse, S.; Chavan-Gautam, P.; Tillu, G.; Mukherjee, A. Mitochondrial resilience and antioxidant defence against HIV-1: unveiling the power of Asparagus racemosus extracts and Shatavarin IV. *Front. Microbiol.* **2024**, *15*.1475457.
(63) Mitra, S. K.; Prakash, N. S.; Sundaram, R. Shatavarins (containing Shatavarin IV) with anticancer activity from the roots of Asparagus racemosus. *Indian J. Pharmacol.* **2012**, *44*, 732−736.
(64) Ganot, N.; Meker, S.; Reytman, L.; Tzubery, A.; Tshuva, E. Y. Anticancer metal complexes: synthesis and cytotoxicity evaluation by the MTT assay. *J. Vis Exp* **2013**, e50767.
(65) Horvath, B.; Marton, Z.; Halmosi, R.; Alexy, T.; Szapary, L.; Vekasi, J.; Biro, Z.; Habon, T.; Kesmarky, G.; Toth, K. In vitro antioxidant properties of pentoxifylline, piracetam, and vinpocetine. *Clin. Neuropharmacol.* **2002**, *25*, 37−42.
(66) Shuchi, S. S.; Trivedi, M.; Tripathi, D.; Pandey-Rai, S.; Pandey, R. Neuromodulatory potential of Asparagus racemosus and its bioactive molecule Shatavarin IV by enhancing synaptic acetylcholine level and nAChR activity. *Neurosci. Lett.* **2021**, *764*, 136294.
(67) Nasr, M.; Wahdan, S. A. Neuroprotective effects of novel nanosystems simultaneously loaded with vinpocetine and piracetam after intranasal administration. *Life Sci.* **2019**, *226*, 117−129.
(68) Setya, S.; Madaan, T.; Razdan, B. K.; Farswan, M.; Talegaonkar, S. Design and Development of Novel Transdermal Nanoemulgel for Alzheimer's Disease: Pharmacokinetic, Pharmacodynamic and Biochemical Investigations. *Curr. Drug Deliv.* **2019**, *16*, 902−912.


https://doi.org/10.1021/acsomega.4c09072
*ACS Omega* 2025, 10, 9132−9153